Materials Science and Engineering, B18 (1993) 237–259

Indium arsenide: a semiconductor for high speed and electro-optical devices

A. G. Milnes
Department of ECE, Carnegie Mellon University, Pittsburgh, PA 15213 (USA)

A. Y. Polyakov
Institute of Rare Metals, Moscow (Russian Federation)

(Received July 2, 1992; in revised form September 3, 1992)

Abstract

Indium arsenide is a direct gap semiconductor (0.36 eV at 300 K and 0.40 eV at 77 K) with high electron mobility (greater than 20 000 $cm^2 V^{-1} s^{-1}$ at 300 K and approximately 60 000 $cm^2 V^{-1} s^{-1}$ at 77 K). The hole mobilities are in the range 100–400 $cm^2 V^{-1} s^{-1}$. Its electro-optical properties are of interest for the IR range out to about 3 μm and to 8 μm in conjunction with In(As,Sb) alloys. Lattice matched heterojunctions can be obtained with alloys such as $Al_xGa_{1-x}As_ySb_{1-y}$. InAs has also been grown on a range of non-lattice-matched semiconductors such as GaSb, InP, GaAs and AlSb, and has exhibited interesting quantum well actions. The field effect transistor (FET) and modulated doped field effect transistor (MODFET) properties are promising but have not been fully developed. The low field for avalanche action (about $10^5 V^{-1} s^{-1}$) presents some device limitations.

1. Physical properties of InAs

InAs has a bandgap of 0.36 eV at room temperature and 0.40 eV at 77 K. The cubic lattice constant is 6.058 Å and therefore is slightly smaller than that of GaSb (6.095 Å) [1, 2] as seen from Fig. 1. For lattice match purposes, alloys of $Al_xGa_{1-x}As_ySb_{1-y}$ are very appropriate, particularly as they form heterojunctions with InAs that are type 2, as may be inferred from Fig. 1(b). In such structures, known as staggered gap, the conduction band edge of the InAs lies in the bandgap region of the AlGaAsSb alloy. However, the lattice-matching alloy of $GaAs_{0.1}Sb_{0.9}$ results in a broken-gap aligned heterojunction and therefore is of lesser inter-est. Numerous quantum well stuctures such as AlSb–InAs, GaSb–InAs, GaInAs–InAs and GaAs–InAs are, of course, of interest for certain specialized applications.

InAs has a melting point of 942 °C which is lower than the 1240 °C melting point of GaAs, but substantially higher than the 712 °C melting point of GaSb. Sirota has presented a review of thermodynamic data for the III–V semiconductors including curves of dissociation vapor pressure versus temperature [3]. The vapor pressure of As_2 and As_4 over InAs at temperatures of interest, such as 400–600 °C, is much larger than for GaAs. The heat of formation of InAs is

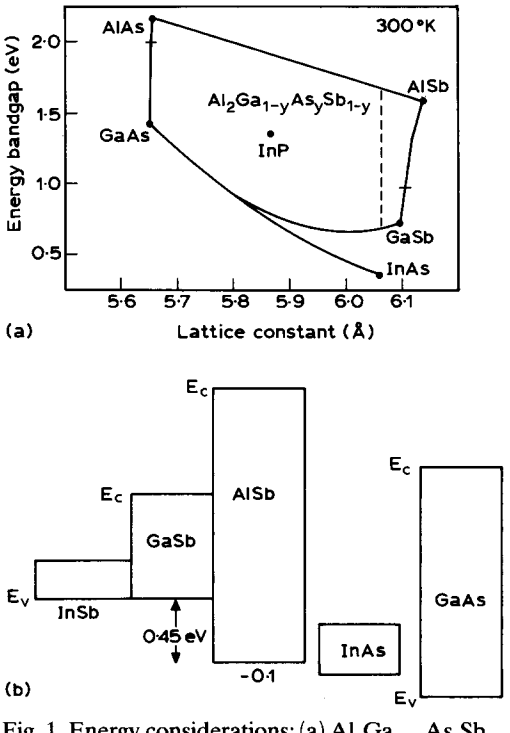

Fig. 1. Energy considerations: (a) $Al_xGa_{1-x}As_ySb_{1-y}$ alloys along the dashed line are lattice matched to InAs [1]; (b) energy-gap line-ups showing how InAs relates to other III–V semiconductors in the formation of staggered-gap and broken-gap heterojunctions.

0921-5107/93/$6.00

lower than for GaAs and comparable with that of GaSb. This sets limits to processing temperatures. For instance, GaAs may be grown by molecular beam epitaxy (MBE) at 550–570 °C but homo-epitaxial InAs is usually grown at 370–430 °C substrate temperatures.

The calculated energy band structure for InAs is shown in Fig. 2. It is seen to be direct-gap [4, 5] at Γ and the L valley minimum is considerably above (0.85 eV) the Γ conduction band minimum, unlike GaAs where the Γ–L spacing is 0.35 eV and GaSb where the spacing is only 0.085 eV. Hence valley transfer effects are not of great significance in InAs although not entirely negligible [6–8].

Undoped InAs is often found to be n-type because of trace impurities such as S. The electron mobility [9] tends to be around 20 000 $cm^2\ V^{-1}s^{-1}$ at room temperature and 60 000 $cm^2\ V^{-1}s^{-1}$ at 77 K, as shown in Fig. 3. As this room temperature mobility is several times that of GaAs this is an interesting plus for InAs. This 20 000 $cm^2\ V^{-1}s^{-1}$ may in fact be limited by surface effects since from phonon scattering considerations, mobility values as high as 30 000 $cm^2\ V^{-1}s^{-1}$ could be expected in bulk InAs crystals. The electron drift velocity at high electric fields is shown in Fig. 4 to be about 2×10^7 cm s^{-1} at 80 K, and shows no valley transfer effect [10]. The Hall mobility for holes in 2×10^{17} cm^{-3} p-type InAs is seen to be about 150 $cm^2\ V^{-1}\ s^{-1}$ at 300 K (Fig. 5), but other measurements suggest values twice as large can be achieved in more perfect material.

Hole doping may be by Zn, Cd, Mg, Be and other elements [12]. Electron doping may be by S, Se, Te or Sn [13–16]. Solubility limits for Te and Zn have been studied by Glazov and Nagiev [17]. Compensation in InAs:Cr [18], InAs:(Zn,S) [19], InAs (Zn,Sn) [20] and

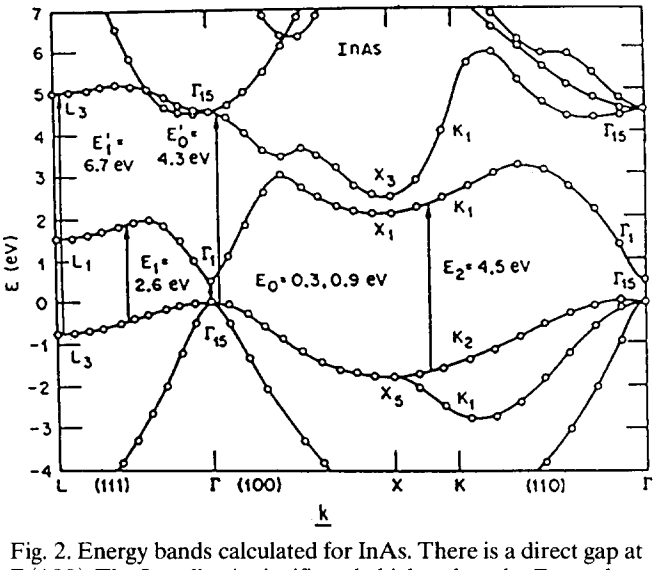

Fig. 2. Energy bands calculated for InAs. There is a direct gap at Γ (100). The L_1 valley is significantly higher than the Γ_1 conduction band valley [5].

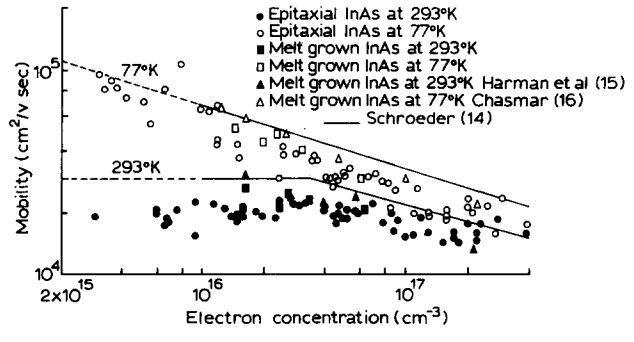

Fig. 3. Electron mobility in InAs as a function of electron concentration [9].

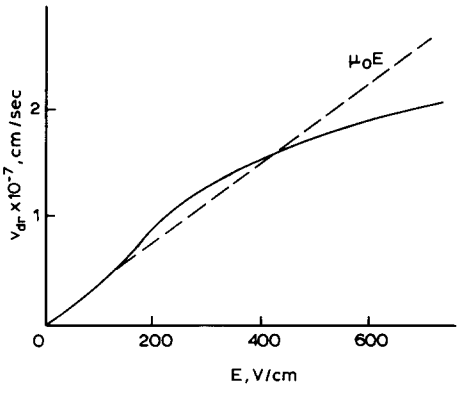

Fig. 4. Dependence of the drift velocity of electrons in n-type InAs on the electric field recorded at $T_0 = 80°$ K for a sample with an electron density $N_e = 1.6 \times 10^{16}$ cm^{-3} and a mobility $\mu_0 = 3.8 \times 10^4$ $cm^2\ V^{-1}\ s^{-1}$. The dashed line represents the field dependence of the product $\mu_0 E$ [10].

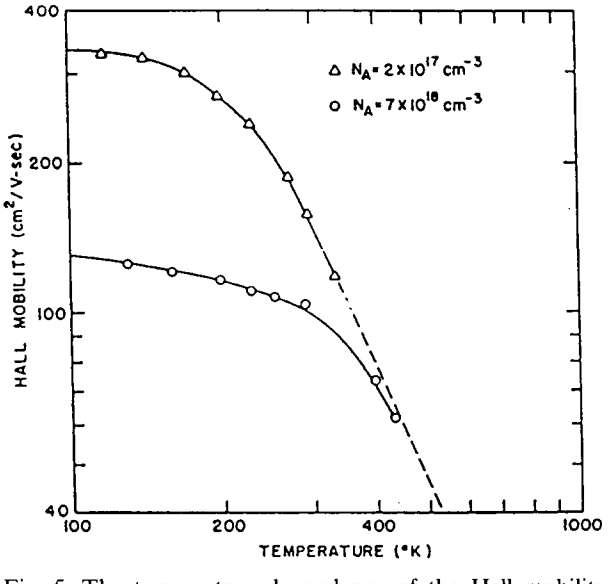

Fig. 5. The temperature dependence of the Hall mobility in p-InAs [11].

InAs (Mn) [21] has been examined. Little has been reported on Si doping in InAs, although this is common for molecular beam epitaxy (MBE) of InGaAs. Nuclear transmutation doping by Sn has been demonstrated in the range 10^{17}–10^{19} cm^3 [22]. Deep levels in InAs films have been studied in metal-insulator semiconductor structures [23].

Because of the high electron mobility, magnetic field effects are strong in InAs, and Hall effect devices were among the earliest applications [24, 25]. A heavy surface accumulation of electrons occurs in InAs, so the Hall coefficients must be interpreted in terms of a two-layer model, with surface and bulk transport actions [26, 27].

The surface accumulation may be as high as the mid-10^{12} electrons per square centimetre, and exhibit effective mass changes. The electrons in the accumulation layer are quantized and show Landau level effects at low temperatures [28–34]. Electron tunneling studies in nInAs–oxide–Pb have provided fundamental information on such effects. The importance of the surface electron accumulation layer in devices is that it is difficult to suppress and it therefore tends to create leakage paths and excess current generation in diodes and transistors of InAs, and alter the Hall behavior in magnetic sensing devices. Some device characteristics that are probably affected by surface leakage current are presented later.

Another aspect of InAs that needs to be considered involves the optical properties. The photoelectric threshold is reported by Gobeli and Allen [35] and optical constants by Seraphin and Bennett [36]. A number of studies exist on photon absorption [37], carrier recombination [38] and photoconductivity [39, 40]. Photoluminescence studies have been reported for bulk material and for films and for interfaces. The small bandgap of InAs makes it suitable for photodetectors in the 1–3 μm range as described later. Such devices may have heterojunction layers and this raises thermal expansion as well as lattice match considerations. From Fig. 6 the thermal expansion coefficient of InAs is seen to lie between that of GaAs and AlAs [41]. This is of interest in considering strain in heterojunctions involving InAs. Such matters are discussed in Sections 3 and 4.

Good oxides with low interface state density and high breakdown field strength, and that are suitable for high temperature processing have not yet been found for InAs structures. In a study of InAs–MIS capacitors, SiO_2, In_2O_3 and Al_2O_3 films were grown, and it was concluded that Al_2O_3 films deposited from aluminum isopropoxide $Al(OC_3H_7)_3$ at 300 °C on (111)B n- and p-InAs gave the best results. The resistivity of Al_2O_3 was 10^{13} ohm-cm and the interface state density was

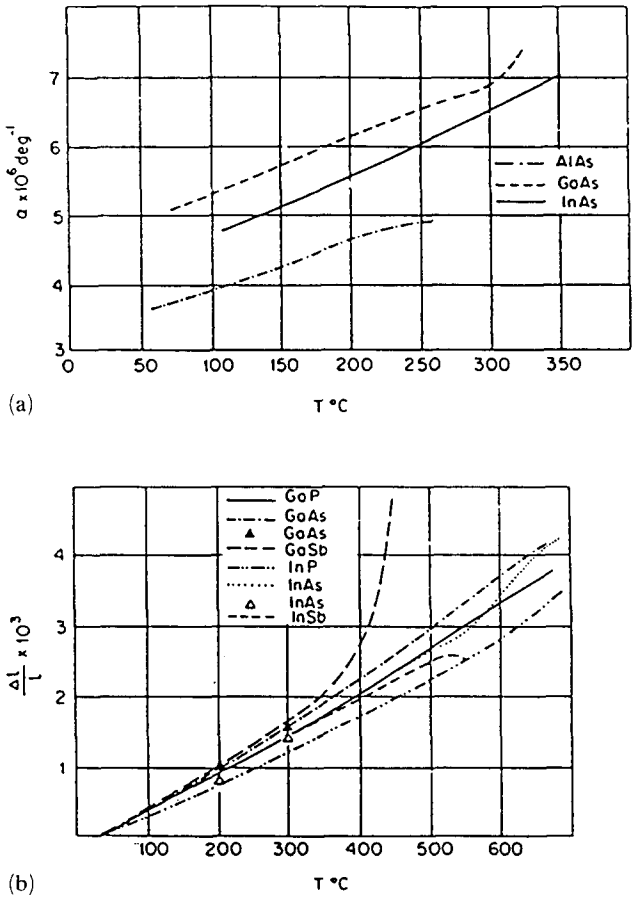

Fig. 6. Thermal expansion for InAs and other semiconductors [41]; (a) the temperature dependence of the linear expansion coefficients for the arsenides of aluminum, gallium, and indium; (b) the relative elongation of the antimonides, arsenides, and phosphides of gallium, and of indium.

10^{11}–10^{12} cm^{-2}. An n-type inversion channel of good surface mobility (5000 cm^2 V^{-1}s^{-1}) was created with a p-type substrate (1.5×10^{17} cm^{-3}) but the transconductance of the fabricated FET device was only 20 mS mm [42, 43]. The causes of the oxide interface states are not known at this time and it is not possible to predict how they might be suppressed. This is a problem facing InAs device designers.

Further discussion of the detailed physics of InAs is not given since considerations of length preclude such matters, and the purpose of the paper is to introduce device concepts to readers who may not be very familiar with InAs. In Section 2 we briefly consider ohmic contacts, Schottky barriers to p-InAs and the behavior of pn junctions of InAs. Heterojunctions involving InAs are discussed in Section 3 and quantum well structures in Section 4. Brief conclusions follow in Section 5.

2. Ohmic, Schottky and homojunction characteristics of InAs

2.1. Ohmic contacts

InAs is a small bandgap semiconductor with electron affinity about 4.9 eV [35] and a tendency to pin the Fermi level of any metal to near the conduction band minimum. Almost any metal therefore makes a quasi-ohmic contact to n-InAs. Figure 7 shows the results of a study of Pt-Ti-InAs (p-type) ohmic contacts [44] which, when sintered at 450 °C, exhibit specific contact resistivities of 10^{-6} ohm cm^{-2}. Most of the multilayer metallurgies that have been developed for contacts to GaAs may be equally effective for InAs although this is unproven and needs study. However there appears to have been no systematic work on the stability of low resistivity contacts to p-InAs, although alloys of In with 5% Cd or Zn have been used [45].

A different concept is the use of an n^+-InAs layer (300 Å thick and mid-10^{19} cm^{-3} Si-doped) on n-GaAs which provides a small barrier to n-GaAs (as shown in Fig. 8) and gives a specific contact resistivity of 10^{-6} ohm cm^{-2}, which is thermally stable for short-term anneals up to 900 °C [46, 47].

2.2. Schottky Barriers

Since the Fermi levels of most metals pin near the conduction band edge, no significant barriers occur for n-InAs. For Au on p-InAs, Schottky barriers can be obtained [48] and Pb has also been used as a barrier material. At liquid nitrogen temperature with a clean interface, an optical barrier height of about 0.30 eV is reported. The effect of a magnetic field is to lower the effective barrier [49]. An interaction between Au and InAs with the evolution of As begins at 300 °C [50].

If the InAs surface is exposed to oxygen Yamaguchi *et al.* [51] have found the surface pinning of thermal oxide on (100) InAs gives a Fermi level above the bottom of the conduction band. This inversion layer action has also been studied for (110) InAs surfaces [52]. Interpretation of the effects of the inversion on the C-V characteristics of Au-p-InAs junctions has been given by Walpole and Nill [53]. From a linear dependence of C^{-2} with voltage, a barrier height of 0.42 eV was obtained at 77 K for $p = 6.3 \times 10^{16}$ cm^{-3}, but the voltage intercept was found to be surprisingly dependent on band-structure parameters, bulk carrier concentration and temperature.

In other studies [54] of Au-p-InAs (6×10^{16} cm^{-3}) with a 2-3 nm thick interface region, a high density of surface states was responsible for surface inversion layers and the barrier height was inferred to be 0.38 eV. Field emission, two-stage tunneling, and thermonic field emission were among the mechanisms needed to interpret the characteristics of Fig. 9.

2.3. Homojunctions

InAs np and pn junctions can be prepared by diffusion or by ion implantation. They may also be prepared by liquid phase epitaxy (LPE), by molecular beam epitaxy (MBE) and vapor-phase epitaxy.

Zn diffusion depths for temperatures 350-500 °C [55] are shown in Fig. 10; a junction depth of 2 μm requires a 2 h diffusion at 400 °C when the substrate is n-type 5×10^{17} cm^{-3} doped.

The I-V characteristics of pn diodes Zn or Cd diffused in 2.5×10^{18} cm^{-3} Te doped InAs [56] with junction depths of 20-50 μm are shown in Fig. 11. The reverse characteristics are poor because of the high doping levels of those diodes, because of an n-inver-

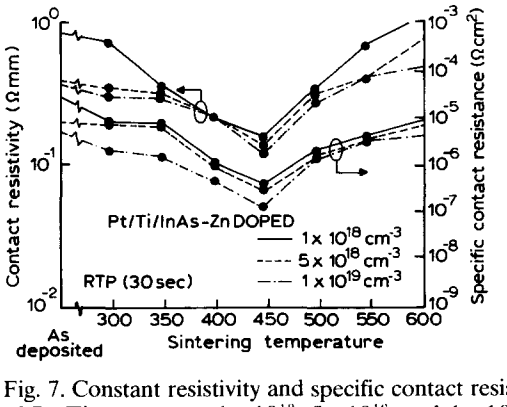

Fig. 7. Constant resistivity and specific contact resistance values of Pt-Ti contacts to 1×10^{18}, 5×10^{18}, and 1×10^{19} cm^{-3} Zn-doped InAs, as a function of the peak rapid thermal anneal temperature [44].

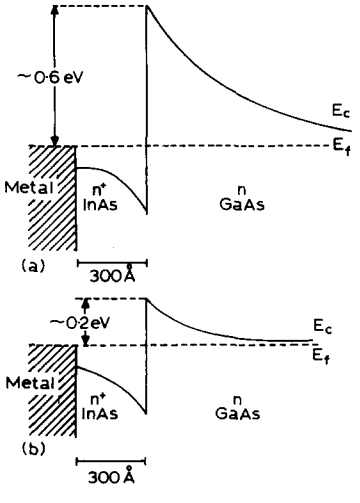

Fig. 8. InAs as a component in an ohmic contact to GaAs. Band diagram of an abrupt InAs-GaAs heterojunction; (a) band diagram expected for a large conduction-band discontinuity or for a heterointerface with a "pinned" Fermi level near midgap; (b) band diagram expected for a small conduction-band discontinuity [46].

sion layer, and also because the critical field strength for avalanche action in InAs is low. This is a feature of InAs, and other small bandgap semiconductors. For simple modeling purposes, the ionization energy may be assumed about equal to one and a half times the energy gap. The curves predicted from this Baraff model are then as shown in Fig. 12(a) [57], where α is the average number of ionizing collisions experienced by an electron in 1 cm of travel in the field direction, λ_R is the mean free path for optical phonon scattering, E is

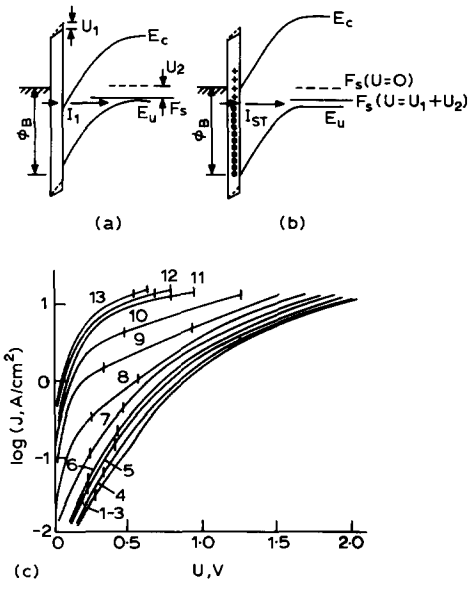

Fig. 9. Energy band diagram and forward current-voltage characteristics for a Au-p-InAs Schottky diode [54]: (a) for $T > 200$ K with $\phi_B > E_g$. I_T is the tunnel current through an inversion region; (b) for 77 K with $\phi_B < E_g$ and I_{ST} is the tunnel current involving surface states; (c) current-voltage characteristics T(K): (1) 77; (2) 89; (3) 110; (4) 133; (5) 156; (6) 175; (7) 194; (8) 221; (9) 229; (10) 244; (11) 259; (12) 273; (13) 298.

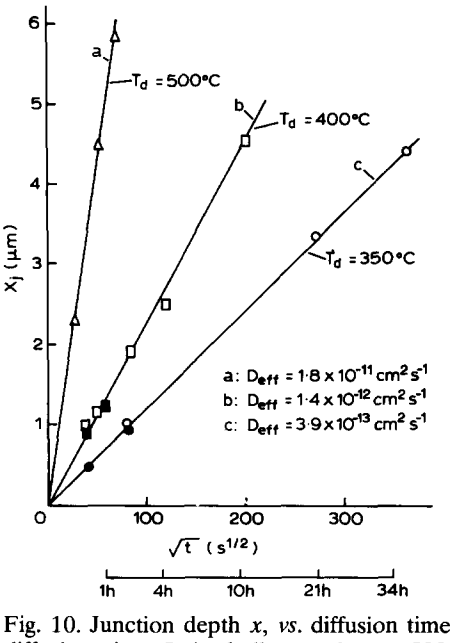

Fig. 10. Junction depth x, *vs.* diffusion time t △, □, ○, for Zn diffusions into InAs bulk samples at 500, 400 and 350 °C, respectively. ■, ● for diffusions into InAsSb epilayers at 400 °C and 350 °C, respectively [55].

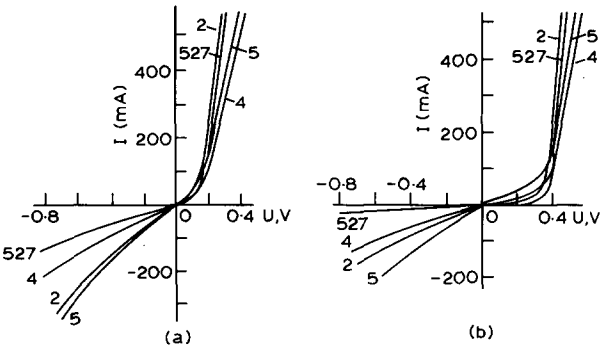

Fig. 11. Current-voltage characteristics of Cd or Zn diffused pn-InAs diodes ($n \sim 3 \times 10^{-18}$ cm^{-3}): (a) for 300 K; (b) for 77 K. Diodes 2–5 are Zn-diffused and 427 and 527 are Cd-diffused. Diffusion depths were in the range 20–50 μm [56].

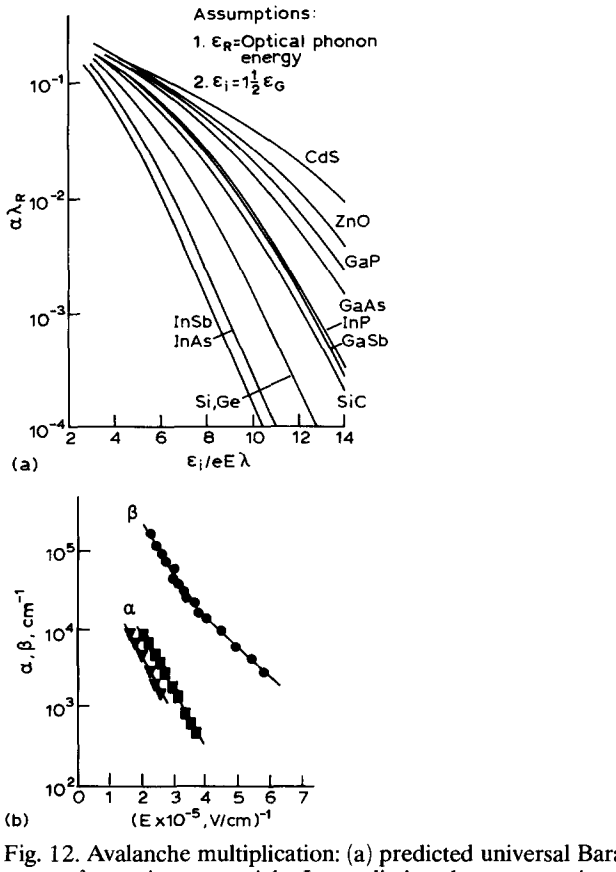

Fig. 12. Avalanche multiplication: (a) predicted universal Baraff curves for various materials. In predicting these curves it was assumed that the ionization energy was equal to 1.5 × the energy gap. The small bandgap, high mobility semiconductors InAs and InSb are seen to have avalanche (related to α) at low electric fields E [57]; (b) electron ionization coefficient α and hole ionization coefficient β for InAs [58].

the field strength in volts per centimetre and λ is the electron mean free path, typically considered equal to λ_R if optical phonon scattering is dominant. λ_R and λ are usually not exactly the same and not well-known for many of the materials. However, it can be inferred from Fig. 12(a) that critical fields strengths for multiplication in InAs will be perhaps a third of that for Si. To confirm this prediction, carrier multiplication in InAs and $In_{0.98}Ga_{0.02}As$ pn junctions was studied by Mikhailova *et al.* [58]. The critical field strength for the onset of multiplication was inferred to be 8×10^4–1.2×10^5 V cm^{-1}, in line with expectations. This critical field corresponds to a reverse voltage of about 4.0 V for an abrupt p^+n diode with $n=4\times10^{16}$ cm^{-3} so useful device behavior is possible. By illuminating the diode from the p- and n-sides separately, it was shown that the hole ionization coefficient β was an order of magnitude higher than the electron ionization coefficient α.

This high ratio is an advantage in the performance of photodiodes that depend on avalanche action. Fig. 12(b) shows the dependence of the ionization coefficients on the peak electric field strengths. A comparison with the Baraff theory yielded the threshold ionization energies of electrons and holes, and their average mean free paths for the scattering by optical phonons: $\varepsilon_{i,e}=0.42$ eV and $\lambda_e=170$ Å, $\varepsilon_{i,h}=0.43$ eV and $\lambda_h=400$ Å. It was concluded that holes from the spin-orbit-split valence band ($\Delta=0.43$ eV in InAs) participated actively in the impact ionization processes.

The Mikhailova pn diodes were created by Cd diffusion. Some diffusion coefficients for various elements in InAs are given in Table 1 [59]. These are from early studies, and very little systematic diffusion work appears to have been done since then.

In heavily compensated InAs the current flow in a bar at high-pulsed fields shows an increase at a field strength at about 10^3 V cm^{-1} as in Fig. 13 [60, 61]. Several mechanisms may be involved in this low field

TABLE 1. Diffusion coefficients (D_0) and activation energies (ΔE) for various elements diffused in InAs (quoted by Kendall [59])

Element	D_0, cm s^{-1}	ΔE, eV	Structure
Mg	1.98×10^{-6}	1.17	pn
Zn	3.11×10^{-3}	1.17	pn,$^+$
Cd	4.25×10^{-4}	1.17	pn
Ge	3.74×10^{-6}	1.17	
Sn	1.49×10^{-6}	1.17	
S	6.78×10^{0}	2.20	np
Se	1.26×10^{1}	2.20	np
Te	3.43×10^{-5}	1.28	np, surface erosion
Cu		0.52	interstitial

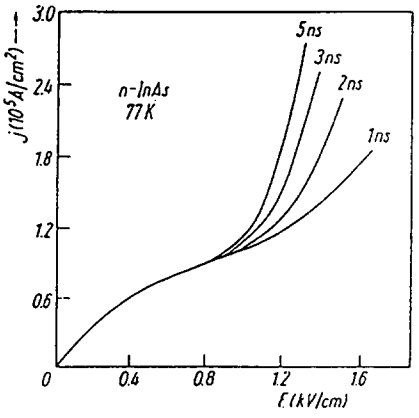

Fig. 13. Current density in an n-InAs bar (77 K) showing current increase setting in at about 1 kV cm depending on pulse length [60].

action, including impact ionization of incompletely ionized defects, the possible presence of impurity banding, possible regions of electric field concentration near the contacts, and surface accumulation effects.

2.4. *Implantation in InAs*

Ion implantation of S in (111) InAs misaligned 7° to minimize possible channeling, has been performed by McNally [62] for infrared detector diodes. The substrates at room temperature were p-type (2×10^{17} cm^{-3}) and the implant voltage was 400 keV. Post implantation annealing was for 1 h at 450 °C in an inert atmosphere. The dose was 8×10^{14} S^+cm^{-2} and this produced peak doping levels of 10^{19} cm^{-3}. The diodes had soft reverse characteristics between 1 V and 2 V. The peak wave length response (77° K) was at 3.1 μm and D* values were in the range 2×10^9–10^{10} cm Hz$^{1/2}$ W^{-1}.

S and Mg implants have been studied by Akimchenko *et al.* [63]. The S doses were in the range 10^{14}–8×10^{14} cm^{-2} with energies 70 keV to 350 keV and the annealing was at 450 °C or 600 °C in an Ar atmosphere. The crystal orientation was (111) and the surface was coated with SiO_2 (0.3 μm) to limit thermal decomposition during annealing. In some specimens the implant was through the SiO_2 film. The substrate was lightly doped p-type (Zn approximately 5×10^{16} cm^{-3}). The S implant layer thickness was about 0.35 μm and there was residual disorder in the layer after annealing. Effective mobility in the n-type layer (1.3×10^{18} cm^{-3}) was about 20 000 cm^2 V^{-1} s^{-1} if the S implantation was through the SiO_2 film and 5000 cm^2 V^{-1} s^{-1} if no film was present. The Mg implants (8.10^{14} cm^{-2}) in n- or p-type InAs (3×10^{16} cm^{-3}, Te) at 350 keV gave effective carrier concentrations of the order of 10^{20} cm^{-3}, but these carriers were n-type because of the formation of donor-type defects [63]. It is clear that more work is needed to achieve successful

p-type implanted layers in InAs. However, perhaps this is not a worthwhile objective in view of the possibility of epitaxial p-type growth.

Since Mg implantation of InAs has created donor type defects, the possibility exists of using non-doping irradiation to create n-layers in pInAs. Proton implantation (100 keV, doses 10^{14}–10^{15} cm^{-2}) into pInAs ($p = 2.10^{17}$ cm^{-3}) was performed and we observed n-type layers with n of the order of 10^{18} cm^{-3} and mobility about 3000 cm^2 V^{-1} s^{-1} (77 K) created. The defects were stable at 200 °C and photosensitive diodes action was observed.

Ar ions implanted at 250 keV have also been shown to convert p-InAs: Mn [64, 65] to n-type [66].

Proton or other defect creating implants to produce np junctions for photodetector arrays, could use photo resists or oxides as masks to define the structure needed, and so may be more convenient than n-type impurity implants that require high temperature activation anneals.

In other studies Guseva *et al.* [38, 67] implanted Si, Ge and Sn at 40 keV into 4.8×10^{16} and 2.5×10^{17} n-type InAs. The behavior is amphoteric and, in addition to the formation of shallow donors, there was also the formation of acceptor levels. From 77 K photoluminescence measurements, the Si^+ ions produced an acceptor level 20 meV above the top of the valence band, and Ge^+ and Sn^+ ions produced levels at 14 meV and 10 meV respectively. Indium arsenide has also been irradiated with fast neutrons [68] to gain better understanding of defect formations. Some defects were not annealed even after 20 min 900 °C heat treatments.

2.5. *Epitaxy of InAs*

Epitaxy may be by liquid phase growth or by molecular-beam epitaxy or by vapor-phase epitaxy. LPE from an In solution at 541 °C on (100) orientated InAs has been studied by Harrison and Houston [69]. Te was found to have a doping capability over 10^{19} cm^{-3} with a large distribution coefficient of 8.4. The relatively high vapor pressure can however be a problem in multiple layer growths. Sn has a small distribution coefficient 1.1×10^{-3} but more than a few percent of Sn in the solution results in poor growths. The largest electron concentration achieved with Sn doping was 2×10^{18} cm^{-3}. The background electron density undoped after extensive bake out of the system was mid 10^{16} cm^{-3}. LPE growth gives layers with low trap densities but requires careful temperature control if thin layers are to be grown. LPE has been used to grow InAs on GaAs and Si [70]. One of the problems with LPE is that, if multiple layers of various compositions are required, the achievement of clean transitions between layers is a difficulty, and other growth methods such as MBE or metal-organic chemical vapor deposition must be considered.

Molecular beam epitaxy of InAs on InAs has been examined by several groups with experiences that have been rather varied, and so merit a brief review here. Foxon and Joyce [71] found the sticking coefficient of As_4 on InAs to be 0.5 for growths at substrate temperatures of 400–480 °C. The transfer to an In stable surface occurred at 447 °C in their system for an As_4 flux of 1.5×10^{13} cm^{-2}. Grange *et al.* [72] who were growing InAs on GaAs using As_4 have some interesting observations on flux ratios for a growth temperature of 370 °C. At this temperature InAs, according to Grange, loses As_2 because of thermal decomposition at 3×10^{12} molecules cm^{-2} s^{-1} irrespective of the incident indium flux. The incident As_4 flux has to compensate for this loss as well as satisfy any arriving In atoms. The As_4 is assumed to dissociate on the (100) surface if In is present and two atoms of As are incorporated for each molecule of As_4. For a flux ratio As_4:In greater than four, the Grange layers were milky. Optimum electrical properties were obtained with the smallest arsenic flux consistent with the decomposition of stoichiometric layers. Grange also remarks that the kinetic theory of gases shows that a chamber background pressure of 6×10^{-6} torr corresponds to an As_4 flux at the substrate of 7×10^{14} molecules cm^{-2} s^{-1}, but claims that there is something in the mechanism of InAs film growth that enables a differentiation between As_4 molecules arriving directly from the source and those that arrive after one or more collisions with the chamber walls. Data on As_2 pressure over InAs appear in [3, 73].

Newstead and coworkers [74, 75] however arrived at considerably different conclusions regarding the permissible flux ratios. They have grown mirror-shiny InAs on (100) InAs under (2×4) and (1×1) reconstructions at As_4:In flux ratios as high as 40:1, and for growth temperatures between 350 °C and 450 °C. For the growth of InAs on GaAs however, they used As_4:In flux ratios between 16 and 20 for a substrate temperature of 530 °C. Similar ratios were used by Yano *et al.* [76].

In other work for the growth of InAs, $AlAs_{0.16}Sb_{0.84}$ and $Al_{0.8}Ga_{0.2}As_{0.14}Sb_{0.86}$ on (100) InAs with As_2 and Sb_2 beams the growth temperature was 425 °C [77]. A beam equivalent pressure ratio P_{As_2}:P_{In} of about three was satisfactory at an In flux of 1.10^{14} atom cm^{-2} s^{-1} for a growth rate of 0.2 μm h^{-1}. Desorption of oxide from the InAs substrates was achieved by heating the substrate to 525 °C for 20 min under an As_2 flux. Schaffer *et al.* [78] preferred In stabilized (4×2) growth conditions with ϕ_{As_4}:$\phi_{In} = 2.3$ and a growth temperature 520 °C for the growth of InAs on GaAs (100). The first stages of MBE growth of InAs on

GaAs have been examined by several groups [79–84] in attempts to understand the nucleation and improve the interface properties. Growths of InAs on GaAs (111)A, (311)A, and (711)A planes have been studied by Kudo *et al.* [85] at 475 °C, however the (100) plane appears to be the most desirable for good growths.

For the growth of $InAs_{1-x}Sb_x$ on (100) InAs Yen and coworkers [86, 87] used a graded composition after a 1 μm buffer layer of InAs was grown. The surface oxide was desorbed at 480 °C in an arsenic pressure of 3×10^{-6} Torr and 480 °C was also the growth temperature for growth rates from 0.2 μm h^{-1} to 1.6 μm h^{-1} under group V stabilization conditions.

Consider now vapor-phase growth in InAs, which has received less attention than MBE growth. Epitaxial InAs has been grown on InAs substrates with (100), (110), (111)A and (111)B orientations by using the reaction of $AsCl_3$ with indium or polycrystalline InAs. Mirror-like surfaces of the grown layers were obtained on (100) and (111)B planes [88]. The undoped layers were n-type and the electron mobility was 170 000 cm^2 V^{-1} s^{-1} at 77 K. Plasma-hydrogen-assisted epitaxial growth of InAs on GaAs, InP and GaSb at 330–530 °C has also produced promising results [89].

Since organometallic vapor-phase epitaxy is well developed for GaAs, this has also been used for InAs growths [90, 91]. The precursors may be trimethylindium or ethyldimethylindium and arsine or tertiarybutylarsine. The dominant impurity is carbon (10^{17} cm^{-3} or greater) which is a donor in the InAs. The growth temperature must be 500 °C–600 °C to limit the carbon density and for good photoluminescence. A laboratory active in MOCVD growth of InAs, InGaAs, InAsSb and GaSb is the Oxford-based group of Walker *et al.* [92–94]. One of the limitations of the MOCVD technology is that it is difficult to grow aluminum-related semiconductors without heavy carbon doping being present. MOCVD is also inclined to produce lateral growth whereas MBE is a direct line-of-sight deposition. This is of significance if localized growth is needed.

3. Heterojunctions involving InAs

3.1. Lattice matching

Alloys of $Al_xGa_{1-x}As_ySb_{1-y}$ that lie along the dashed line in Fig. 1(a) are compounds of interest for lattice-matched growth on InAs substrates. These cover a wide bandgap range, and in principle one such film grown on InAs could be capped by a second composition, also lattice matched, so that many heterojunction combinations are conceptually possible. Other alloys of interest are quaternaries containing In, namely $Ga_xIn_{1-x}As_ySb_{1-y}$.

Alloys that would be lattice-matched to InAs (6.058 Å. Eg = 0.36 eV) may be predicted from the theoretical studies of Glisson *et al.* [95], Williams *et al.* [96] and Adachi [97]. Examples of such alloys are given in Table 2. All would be lattice-matched to each other and to the substrate to about 10^{-3} and those below 1.2 eV have direct bandgaps. Fig. 14(a) shows the bandgap energies for the quaternaries $Ga_xIn_{1-x}As_ySb_{1-y}$ lattice-matched to InAs. The bandgap range (direct) is seen to be 0.36 eV to 0.69 eV (3.4 μm to 1.8 μm). The arsenic fraction needed for lattice matching is given by Adachi as:

$$y=\frac{0.4210-0.3835x}{0.4210+0.0216x} \qquad 0<x<1.0 \qquad (1)$$

In Fig. 14(b) bandgap energies for the quaternaries $Al_xGa_{1-x}As_ySb_{1-y}$ are shown. The range is from 0.7 eV to 1.7 eV with a direct-to-indirect transition at $x=0.45$. The expression relating y to x for a lattice-match to InAs is:

$$y=\frac{0.0375+0.0396x}{0.4426+0.0318x} \qquad 0<x<1.0 \qquad (2)$$

Adachi has also given refractive index data for a range of alloys, and this is of importance if heterojunction barriers are used for optical (and electrical) confinement in injection lasers and other electro-optical devices.

The degree of lattice match is important in heterojunctions (except for very thin strained layer quantum-well type structures) since this determines the quality of the interface [98]. The ΔE_c or ΔE_v values are also

TABLE 2. Examples of alloys that are lattice-matched* to InAs (calculated from eqns (1) and (2))

Band Gap eV (300 K)	Composition
0.36	InAs
0.5	$Ga_{0.5}In_{0.5}As_{0.53}Sb_{0.47}$
0.57	$Ga_{0.7}In_{0.3}As_{0.35}Sb_{0.65}$
0.66	$Ga_{0.87}In_{0.13}As_{0.2}Sb_{0.8}$
0.7	$GaAs_{0.085}Sb_{0.915}$
0.6	$Al_{0.17}In_{0.83}As_{0.84}Sb_{0.16}$
0.8	$Al_{0.29}In_{0.71}As_{0.75}Sb_{0.25}$
1.0	$Al_{0.4}In_{0.60}As_{0.65}Sb_{0.35}$
1.2	$Al_{0.49}In_{0.51}As_{0.57}Sb_{0.43}$
0.8	$Al_{0.07}Ga_{0.93}As_{0.08}Sb_{0.92}$
1.0	$Al_{0.19}Ga_{0.81}As_{0.10}Sb_{0.90}$
1.2	$Al_{0.33}Ga_{0.67}As_{0.11}Sb_{0.89}$

*Slight adjustments of these compositions may be needed for optimum lattice matching since thermal expansion effects during and after growth are not taken into account.

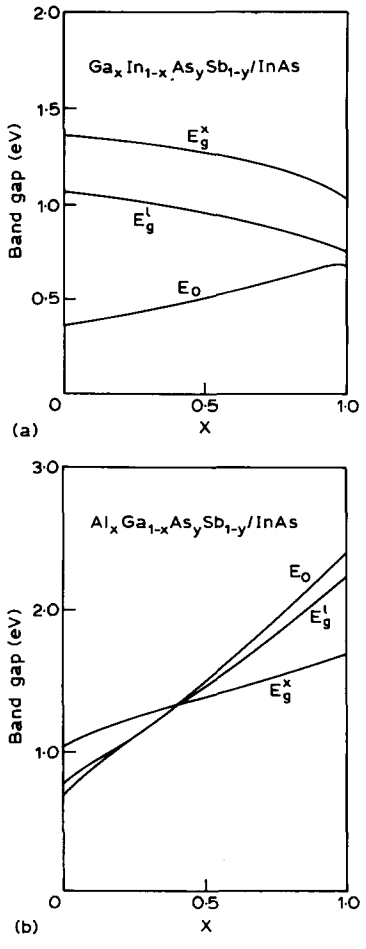

Fig. 14. Bandgap energies *vs.* composition for quaternaries matched to InAs [97]: (a) for $Ga_xIn_{1-x}As_ySb_{1-y}$ lattice-matched to InAs; (b) for $Al_xGa_{1-x}As_ySb_{1-y}$ lattice-matched to InAs.

important unless the interfaces are graded in composition. The ΔE_v line-ups for InSb, GaSb, AlSb, InAs, and GaAs are shown in Fig. 1(b). The ΔE_c or ΔE_v values determined by a variety of measurement techniques [99, 100] are usually found to be correct within ± 0.05 eV. However, these binary semiconductors are not lattice-matched to each other, as may be seen from Fig. 1. Furthermore, it is seen that for InSb–InAs and GaSb–InAs, the line-ups result in broken-gap heterojunctions with the conduction band edge of InAs below the valence band edge of InSb and GaSb. This results in tunneling actions that may or may not be of device interest.

In a first-order model the dangling bonds at the interface of (100) cubic semiconductors of lattice constants a_1 and a_2 are calculated from:

$$N_{DB} = 4(a_1^{-2} - a_2^{-2}) \quad (3)$$

where N_{DB} may be considered representative of the expected interface state density. For a lattice mismatch of as little as 10^{-3} the interface state density may be greater than 10^{12} cm^{-2}, which is sufficient to dominate the electric properties. This simple model neglects the complication of interface mixing at the atomic level [101] and self-satisfaction of bonds. Also it does not consider the fact that thermal expansion coefficients of the compounds are not identical and therefore lattice matching at the growth temperature may involve strain at normal use temperatures [41]. A high degree of composition control and related time-consuming experimentation is therefore usually needed to achieve compromises for the best interface conditions. In high-injection-current devices, such as lasers, where substantial power is involved and temperatures must be kept low, there may also be a need to consider the thermal resistance of the quaternary layers that are greater than for binary layers [102].

Lattice-matching requires the capability for excellent growth control of compositions of quaternary alloys. The problem is complicated by the fact that compositional analysis to the required level is not easily achieved. Bithell and Stobbs [103] state that no technique provides $Al_xGa_{1-x}Sb$ alloy composition to an accuracy better than ± 0.05 in x. Growths therefore tend to involve much reiteration to achieve desired results. Nevertheless well-matched junctions of InAs and related quaternaries have been achieved as in Table 3 [77, 104].

When binary or ternary alloys are grown that are lattice mismatched, the strain can be considerable and there is a critical layer thickness, often about 100 Å, beyond which relaxation of the energy occurs by the development of dislocations and other disorder in the layer. There is the extra complication that strain tends to alter the band structure of the InAs and the quaternary [105, 106]. This is discussed further when we consider quantum well structures involving InAs.

Fairly extensive studies have been made of the growth of InAs on GaAs. In Fig. 1(a) it is seen that there is a considerable lattice mismatch (7.1%) between the two materials. From Fig. 1(b) a substantial ΔE_c barrier (0.90 eV) is expected and ΔE_v is smaller (0.17 eV) [100]. The large lattice mismatch between these materials causes a high density of misfit dislocations to form at or near the interface [107]. The threading components of the misfit dislocations propagate into the epitaxial layer and their density is found to be inversely proportional to the epilayer thickness. This reduction in dislocation density, within the initial few microns, is attributed to dislocation interaction. After about 4 μm of growth the threading dislocation density in one study was of the order of 10^8 cm^{-2}, however bulk-like room temperature mobilities were obtained for Sn-doped InAs layers (22 000 cm^2 V^{-1} s^{-1} for a carrier concentration 5×10^{16} cm^{-3}). The minority carrier properties of the layers were presumably not impres-

TABLE 3. MBE grown $Al_xGa_{1-x}As_ySb_{1-y}$ epitaxial layers on InAs. The material composition was determined by X-ray diffraction and Al–Ga flux ratio measurements. The energy bandgap (E_g) is defined to be at the peak absorption of the photoluminescence (PL) spectrum (from ref. 77)

Composition	PL E_g (meV) 4 K	Line width (meV) 4 K	Comment
$AlAs_{0.16}Sb_{0.84}$	1635	7	Lattice matched
$Al_{0.8}Ga_{0.2}As_{0.14}Sb_{0.86}$	1525	20	Lattice matched
$Al_{0.6}Ga_{0.4}As_{0.19}Sb_{0.81}$	1382	21	Lattice matched
$Al_{0.4}Ga_{0.6}As_{0.19}Sb_{0.81}$	—	—	Lattice mismatched
$Al_{0.2}Ga_{0.8}As_{0.22}Sb_{0.78}$	—	—	Lattice mismatched
$GaAs_{0.23}Sb_{0.77}$	—	—	Lattice mismatched
$Al_{0.5}Ga_{0.5}As_{0.11}Sb_{0.89}$	—	—	Lattice mismatched
$Al_{0.2}Ga_{0.8}As_{0.13}Sb_{0.87}$	—	—	Lattice mismatched
$Al_{0.4}Ga_{0.6}As_{0.11}Sb_{0.89}$	1176	20[a]	Lattice matched
$Al_{0.2}Ga_{0.8}As_{0.1}Sb_{0.9}$	965	9[a]	Lattice matched

[a]Data measured at 8 K.

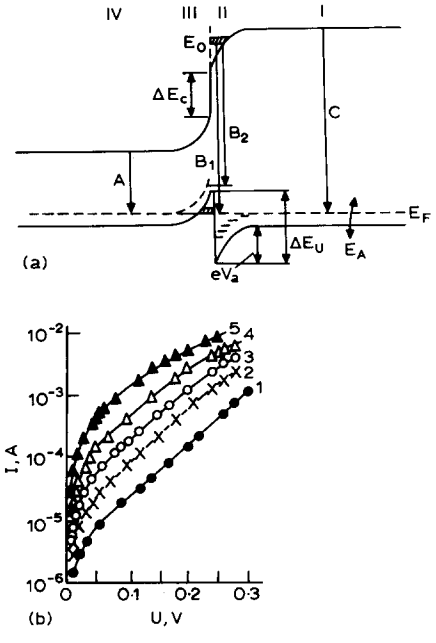

Fig. 15. Heterojunction pp energy band diagram and some p-n current voltage characteristics: (a) energy band diagram of a p-InAs-P-$InAs_{0.63}P_{0.25}Sb_{0.12}$ heterojunction. I is the epitaxial P-InAsPSb layer; II is the depletion layer; III is the space charge layer; IV is the p-type InAs substrate. The arrows labeled A, B_1, B_2, and C represent optical transitions [108]; (b) forward current-voltage characteristics for a p-InAs-n$Al_xGa_{1-x}Sb$ heterojunction recorded at T (K): (1) 290; (2) 323; (3) 344; (4) 369; (5) 395 [109].

sive in view of the dislocation density observed. $Ga_{1-x}In_xAs$ grown on GaAs however has given good FET (and MODFET) properties if x is below 0.3 since the electron mobility is higher than for GaAs in spite of the lattice mismatch.

A p-InAs–P-$InAs_{0.63}P_{0.25}Sb_{0.12}$ heterojunction diagram is shown in Fig. 15(a), and Fig. 15(b) shows characteristics for an InAs–$Al_xGa_{1-x}Sb$ heterojunction. Figure 16 shows how the ΔE_c may be expected to vary with (GaIn)As and (AlIn)As alloy composition.

The energy band offsets in heterojunctions can be modified by the presence of a thin interface layer [111] or by delta doping. For instance, if an n-GaAs layer is provided with a p-delta-doped GaAs layer (10 nm wide, with 2.10^{13} cm^{-2} Be) and this is followed by the growth of n-InAs the ΔE_c and ΔE_v values observed are 0.72 eV and 0.34 eV respectively (compared with the normal 0.90 eV and 0.17 eV) [112]. Raman spectroscopy can be used to characterize the strain when InAs is grown on mismatched substrates, as can double-crystal X-ray diffraction [113].

InAs has been observed to grow to several monolayers of thickness on InP (100) surfaces if the InP surface is arsenic-stabilized [114]. InAsSbP has been grown on InAs, and injection and cathodoluminescence studied [115, 116]. Strain affects both injection and cathodoluminescence.

Alloy clustering may occur in the growth of various alloys (such as InAlAs). For common anion alloy systems for which thermodynamics favor phase separation, the conditions for high-quality alloy and high-quality surfaces (and heterointerfaces) are incompatible if the conventional MBE growth approach is used [117]. The short-range ordering may have effects on both optical and transport properties.

3.2. Optical properties and detectors

The photon absorption coefficient for InAs is given with that of other semiconductors in Fig. 17. The refractive index of InAs is 3.54 (from a relative dielectric constant of 12.5). Adachi has calculated the refractive indices of various quaternary alloys (AlGaAsSb, GaInAsSb and InPAsSb) that may be used as heterojunctions with InAs [97]. These indices are of

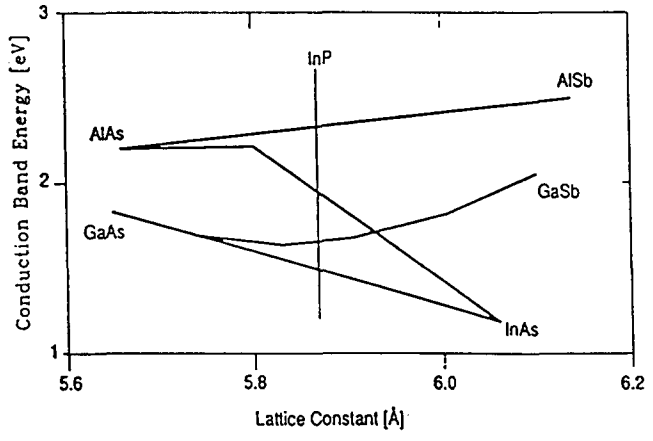

Fig. 16. Graph of conduction-band energies *vs.* lattice constant for the ternary III-V compound semiconductors GaAsSb, GaInAs, AlInAs, and AlAsSb. The energy levels are referenced to the valence-band energy of AlAs [110].

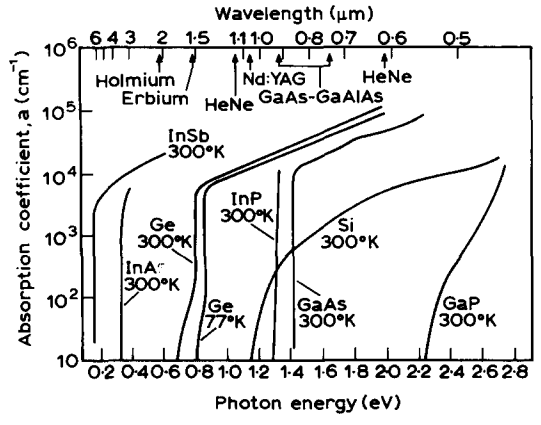

Fig. 17. Absorption coefficients for selected semiconductors in the visible and near-infrared spectral region: InSb, InAs, Ge, Si, InP, GaAs, and GaP. Also shown are the emission energies of some lasers in the same spectral region [122]. InAs is seen to have a direct-gap rise of absorption coefficient.

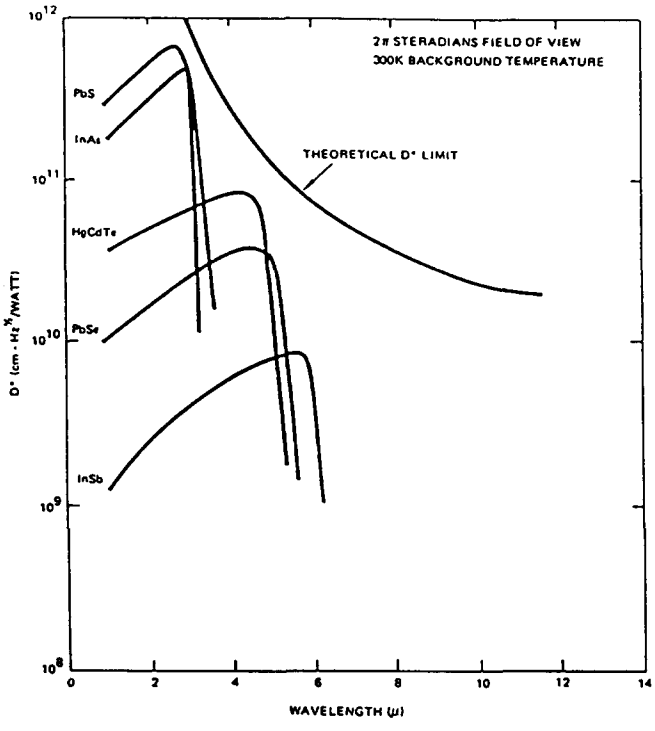

Fig. 18. Representative curves of D^* for four commercial photodetectors operated at 200 K. The theoretical curve gives the limit for D^* with a 300 K background radiation [119, 120].

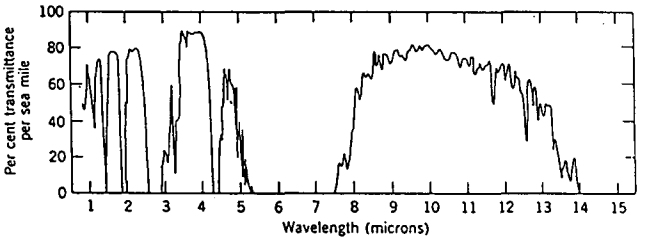

Fig. 19. Atmospheric transmission spectrum, showing windows from 2–2.6 μm, 3.4–4.2 μm, 4.5–5.0 μm, and 8–13 μm. (After Kruse, McGlauchlin, and McQuistan. Reprinted from *Elements of Infrared Technology; Generation, Transmission, and Detection*, John Wiley & Sons, NY., 1962, p. 164).

use in considering optical confinement devices such as lasers and waveguides.

The photodiode, photoconductivity and phototransistor action of semiconductor light detectors have been discussed by many authors [118–123] and figures of merit, such as the sensitivity-to-noise ratio D^*, defined. The D^* value for InAs is high in relation to other photoconductive detectors, as can be seen from Fig. 18. The cut-off of sensitivity at about 3.5 μm wavelength is determined by the bandgap of InAs, and is about the same for Schottky diodes (Au-p-InAs [48]) and pn-InAs diodes. Transmission of IR radiation through the atmosphere [124] is shown in Fig. 19. InAs is a satisfactory detector for the 2–2.6 μm transmission range, but a lower bandgap detector is preferable to cover the 3.4–4.2 μm and 4.5–5.0 μm ranges [125]. InSb will cover these ranges but the detector leakage currents are large unless the temperature is low (77 K or below). An alternative approach, although not one that solves the leakage current problem, is the growth of $InAs_{1-x}Sb_x$ (where x is in the range 0.6–0.8). These alloys result in bandgaps down to 0.15 eV at 77 K [126] because of the composition and the strain in the heterojunction, Fig. 20. An $InAs_{0.15}Sb_{0.85}$–InSb strained-layer superlattice photon detector with $D^* > 1 \times 10^{10}$ cm $Hz^{1/2}$ W^{-1} for wavelengths less than 10 μm has been described by Kurtz and coworkers [127, 128]. Lateral photoconductive superlattice detectors of $InAs_{0.11}Sb_{0.89}$–InSb can exhibit gains as large as 90 since the photocarrier lifetime can exceed the transit time because the barriers (staggered type) can

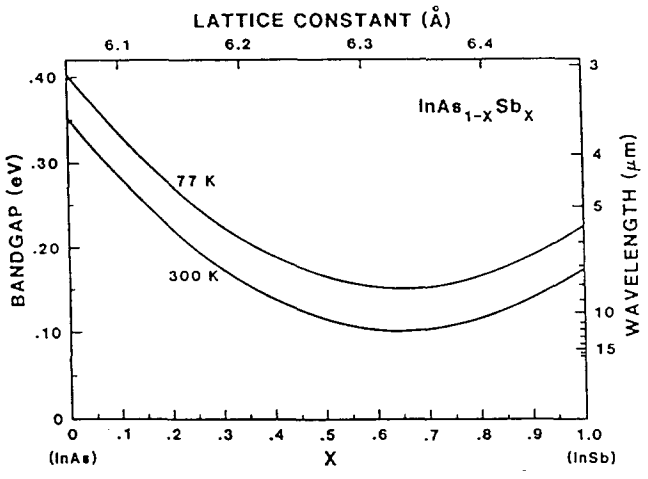

Fig. 20. Variation of the bandgap energy as a function of composition and lattice constant for the InAs–InSb pseudo-binary system at 300 K and 77 K [126].

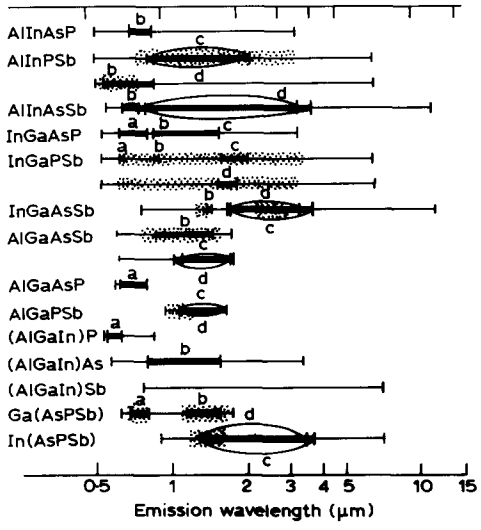

Fig. 21. Expected emission wavelengths for various III–V quaternaries at 300 K. The solid portion denotes the compositions lattice-matched to stable binary crystals: (a) GaAs; (b) GaSb; (d) InAs; shaded areas correspond to the miscibility gaps [136].

suppress the recombination because of the spatial separation of electrons and holes.

A proposal has also been made for an In (As, Sb) sawtooth doping superlattice detector [129] that should be suitable at 77 K for the range 8–12 μm. The superlattice is to be p- and n-delta-doped $InAs_{0.4}Sb_{0.6}$ to improve the photon absorption, which is usually a significant problem in superlattices which, because of the difficulties of sustaining perfect growths, are typically less than 2 μm in total thickness.

Information on charge-coupled area image sensors of InAs was not found in the literature although CCDs and other related devices of InSb were fabricated many years ago [130].

3.3. Injection lasers involving InAs

In early work, Melngailis and Rediker [131] showed that InAs pn diodes would lase near 3.1 μm (band-to-acceptor line at 11 K) with an external quantum efficiency of 12% and a threshold current density of 300 A cm^{-2}. LPE grown pn InAs diode lasers were subsequently fabricated and shown to operate under pulse conditions (0.5 μs pulses) at 77 K with threshold current densities of 2000 A cm^{-2} [132]. The non-radiative lifetime for electrons injected into the p-region was inferred to be 1–2 ns. In other work [133] the delay time of a pulse of light was found to be in the range 6–33 ns. Magnetic fields have some effect on the performance of InAs diode lasers [56].

For two decades since this time, there has been very little work on InAs as the active layer in injection lasers, however H. K. Choi and S. J. Eglash's group is now developing this general area [134]. The work of this group has primarily been with GaInAsSb as the active layer for emission at about 2.2 μm [135], and has achieved threshold current densities as low as 260 A cm^{-2} for a 100 μm wide laser. In preparation however, are active layer InAsSb lasers for 4.0 μm with CW operation up to 80 K and pulsed operation up to 155 K.

The lattice-matched heterojunction possibilities are quite numerous for such materials [136] as can be seen from Fig. 21. With molecular beam epitaxy, good confinement barriers are obtainable. Although non-radiative recombination may be significant in InAs, recent work suggests that it may not be a really serious problem at 77 K. It appears that the main problem is that the effort and funding needed to explore fully the potential of InAs lasers has not been forthcoming.

3.4. FET InAs transistors

The high electron mobility of InAs is a feature of exceptional interest. At 300 K the mobility may be 20 000–25 000 $cm^2\ V^{-1}\ s^{-1}$ and at 77 K values of μ_n of 60 000–80 000 $cm^2\ V^{-1}\ s^{-1}$ have been reported for impurity concentrations of 5×10^{15} cm^{-3} to 10^{16} cm^{-3} with corresponding hole mobilities of about 600 $cm^2\ V^{-1}\ s^{-1}$. Because of the small bandgap of InAs, the intrinsic electron and hole concentrations at 300 K may be expected to be about 10^{15} cm^{-3}, and the resistivity about 0.2–0.02 ohm-cm. The minority carrier lifetime for n-type InAs is about 10^{-8} s and the surface recombination velocity appears to be small (10^3–10^4 cm^{-1} s) although neither of these quantities have received much study. InAs therefore has potential as a semiconductor for room temperature operation but its real forte is at reduced temperatures in the range 200

K to 77 K where it becomes a very interesting semiconductor. The potential exists for very high speed FETs and MODFETs of InAs at 77 K, and two-dimensional electron gas conditions have been created in InAs in preliminary work. A special comment to be made here is that InAs's mobility of 60 000 $cm^2\ V^{-1}\ s-1$ at a doping of $10^{16}\ cm^{-3}$, even without the two-dimensional electron gas structure, is somewhat comparable to the effective 77 K mobility of 60 000 to 70 000 $cm^{-2}\ V^{-1}\ s^{-1}$ for two-dimensional electron gas in GaAs inferred from GaAs–AlGaAs MODFET performance. The high two-dimensional gas mobilities (of order of 200 000 $cm^2\ V^{-1}\ s^{-1}$) reported for GaAs films at 77 K degrade even at moderate fields and are not representative of effective mobilities that can actually be achieved in MODFETs.

The potential high frequency performance of submicrometer gate length FETs has been the subject of a study by Cappy *et al.* [137]. They postulate that the channel transit time will be low if the electrons remain in the low mass valley. This conclusion is satisfied if the average energy of the electrons in the gate-drain space is lower than the intervalley gap $\Delta E_{\Gamma L}$. In a simplified approach then:

$$\Delta E_{\Gamma L} = qEL_g = qV_{Lg} \tag{4}$$

where E is the average electric field under the gate and V_{Lg} the voltage across the gate. Moreover, the average drift velocity is given by:

$$v = L_g/\tau = \mu_0 E \tag{5}$$

and finally:

$$\tau = qL_g^2/\mu_0 \Delta E_{\Gamma L} \tag{6}$$

Therefore in order to minimize the transit time, three parameters are of primary importance: the gate length, the low-field mobility, and the intervalley gap. So materials such as $Ga_{0.47}In_{0.53}As$ or InAs with a high mobility, and possessing a large intervalley gap, may give a small transit time. For GaAs and InP, the products $\mu_0 \Delta E_{\Gamma L}$ are roughly the same (Table 4) and much lower than that for the InAs-related materials. The Cappy study was then extended to a Monte Carlo simulation to obtain the gain-bandwidths and transit times shown in Fig. 22. It is seen that InAs is potentially better than GaInAs for gate lengths 1 μm or less. However InAs FETs have not yet been developed to anywhere near the performance projected in Fig. 22, since very little effort has been applied in this direction.

In 1968 work, thin film FETs of InAs evaporated on glass were examined [138, 139]. The evaporated and heat-treated films were 750–3000 Å thick, and showed an electron concentration of $8 \times 10^{16}\ cm^{-3}$. The FET gate material was Al or Au and the channel length was 10^{-2} cm and the width 0.15 cm. The insulator under the gate was a mixture of SiO and SiO_2 and the thick-

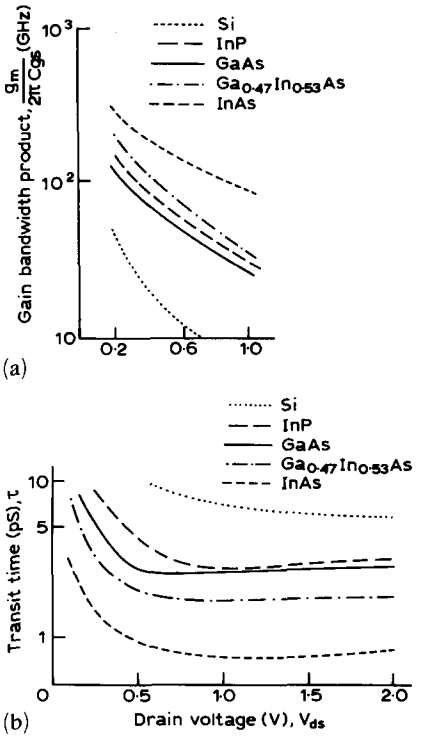

Fig. 22. Predictions of the performance of field-effect transistors of various semiconductors [137]: (a) gain-bandwidth product *vs.* gate length; (b) transit time against drain-to-source voltage. InAs and $Ga_{0.47}In_{0.53}As$ are seen to out perform GaAs.

TABLE 4. Parameters used in the calculation of the FET performance potential of InAs and other semiconductors [137]. $\mu_0 \Delta E_{\Gamma L}$ is a simplified figure of merit for high frequency performance

	m_Γ/m_0	$\mu_0\ cm^2\ V^{-1}\ s^{-1}$	$v_p\ 10^7\ cm\ s^{-1}$	$\Delta E_{\Gamma L}$ eV	E_g eV	$\mu_0 \Delta E_{\Gamma L}\ cm^2\ s^{-1}$
Si	0.27	700	—	—	1.12	—
GaAs	0.063	4600	1.8	0.33	1.42	1520
InP	0.08	2800	2.4	0.61	1.35	1680
$Ga_{0.47}In_{0.53}As$[a]	0.032	7800	2.1	0.61	0.78	4760
InAs	0.022	16000	3.5	0.87	0.35	13900

[a]This alloy composition is a lattice match to InP.

ness 0.3 μm. The maximum transconductance observed was 5.5 mS and the field effect mobility was about 2800 $cm^2\ V^{-1}\ s^{-1}$ at 300 K. The crystallites in the film after grain growth were larger than the channel length so the best FETs were single crystal, or nearly so. In another early study of InAs FETs, the insulator was Al_2O_3 [42, 43] on bulk n-InAs. The channel length was 40 μm and the width was 110 μm. The transconductance of the n-type inversion layer was about 20 mS mm^{-1} and the channel mobility 5000 $cm^2\ V^{-1}\ s^{-1}$. A superior insulator–InAs technology must be discovered if this performance is to be further improved.

In more recent work [140] a heterojunction structure, Fig. 23, was used instead of an MIS structure. The $Al_{0.5}Ga_{0.5}Sb$ 150 Å layer and the 60 Å AlSb layer supply electrons to the InAs channel. The GaSb cap layer has a 0.5 eV barrier for holes but may tend to act as a gate "metal". For a gate length of 1.7 μm the transductances were in the 400–500 mS mm^{-1} range and

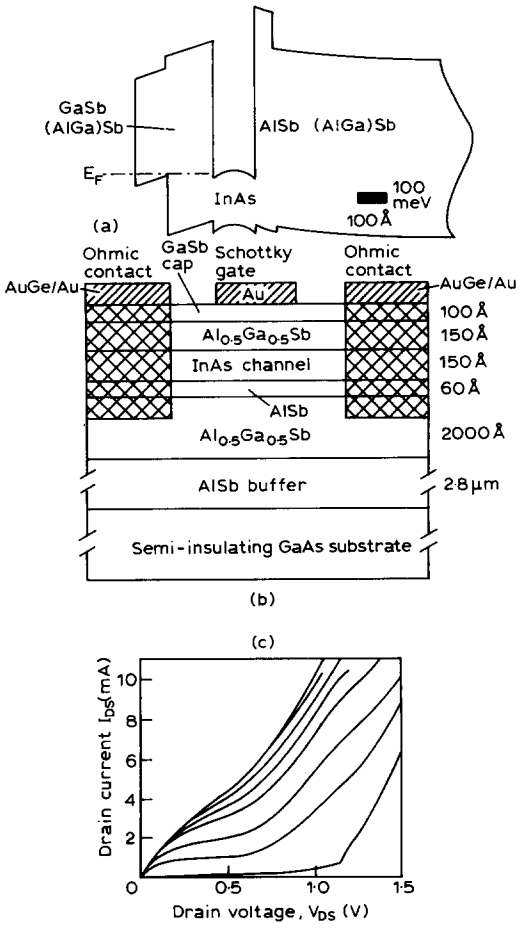

Fig. 23. InAs FET with (AlGa)Sb and AlSb barriers [140]: (a) energy-band diagram; (b) structure schematic; (c) measured drain current characteristics of the 1.7 μm (gate length) InAs FET at 300 K. The gate voltages are taken from −0.1 V to 0.25 V in 50 mV steps.

the K factor ($\delta g_m/2\delta V_g$) was 1450 mS $V^{-1}\ mm^{-1}$ (at $V_{ds} = 1$ V) at room temperature. A kink effect is seen in the current–voltage characteristics. Similar effects are observed in very short-channel MODFET and silicon-on-insulator (SOI) types of devices. Common features of these devices are electrically floating substrates, and existence of electrons with energy high enough to create excess carriers by impact ionization; the impact ionization in the relatively long-gate-length (1.7 μm) devices reflects the narrow bandgap energy of InAs. However, in general these results indicate the potential superiority of InAs channel FETs over (InGa)As or GaAs channel FETs.

In other work [141], an InAs FET has been fabricated in which the gate has no intermediate layer between it and the channel. The separation of gate and channel carriers is achieved by using the staggered band alignment of InAs–(AlGa)Sb such that a p^+ (AlGa)Sb gate layer is placed in direct contact with the n-type InAs channel. The structure and its characteristics are shown in Fig. 24 and it has been termed a zero-insulator-thickness FET, or ZFET. The device is not suitable for room temperature operation but at 77 K transconductances of 500 mS mm^{-1} have been observed.

Since the electron mobility performance of InAs n-channel FETs is promising it has been proposed that they could form a complementary pair with a p-channel GaSb FET that has good hole mobility [142]. The prediction is that the room temperature performance could be several times greater than for AlGaAs–GaAs complementary pairs because of the superior barrier and mobility conditions. Some complementary pair studies have been attempted [143] but the work is quite preliminary. Gallium antimonide device properties have been reviewed recently [144, 145] and GaSb FETs discussed that might form part of the complementary pair. A two dimensional simulation of a 77 K 0.25 μm Schottky gate InAs FET has suggested that the device could have performance characteristics comparable even to Josephson junctions for high-speed low-power logic applications.

Although the performances achieved so far for InAs FETs are not that impressive, further development to improve channel and gate properties, and to minimize parasitics, should be rewarding. In particular, the parasitic channels associated with surface n-type inversion must be controlled in the designs.

3.5. Hot electron transistors involving InAs

Another aspect of InAs that is of interest is that for $n = 1 \times 10^{16}$ cm^{-3} the electron mean free path is believed from limited studies to be about 200 Å for electrons, say, 0.3–0.4 eV above the conduction band minimum [58]. Therefore, hot electron transistors are

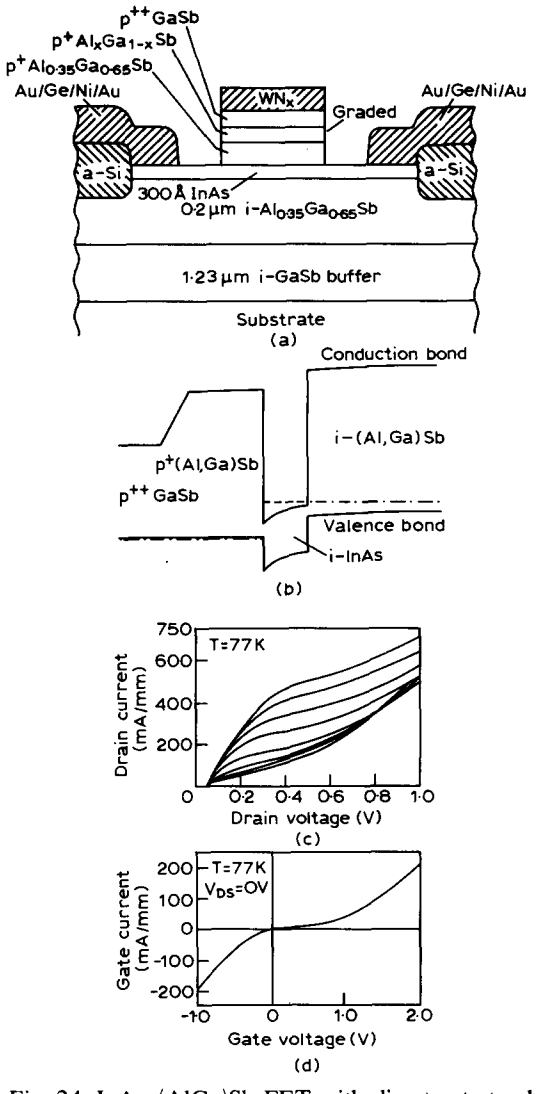

Fig. 24. InAs–(AlGa)Sb FET with direct gate-to-channel contact for 77 K operation [141]: (a) schematic cross-section; (b) band-edge diagram with the gate (p^{++}GaSb, p^{+}(AlGa)Sb) shown biased 0.3 V relative to the channel; (c) drain current *vs.* drain voltage for a 1 μm ZFET at 77 K. Gate width is 20 μm. The gate voltage from 0.3 V to 1.8 V in 0.15 V steps; (d) gate leakage current for the same ZFET, also at 77 K.

possible with InAs base widths of 100 Å or so. Among the materials that might be used as the launching emitter are AlSb, GaAlSb, and GaSb. The collector material may be selected to have a lower barrier height to aid in the collection process, as shown in Fig. 25. Current *vs.* base-emitter voltages for these structures are shown in Fig. 26(a) and the collector characteristics in Fig. 26(b). The curves are free of kinks but the current gain (common emitter) is only six for a base-width of 100 Å and the current rises considerably as the collector-emitter voltage increases, so the FET has a low output impedance. Quantum reflections at the collector are considered responsible for the low gain,

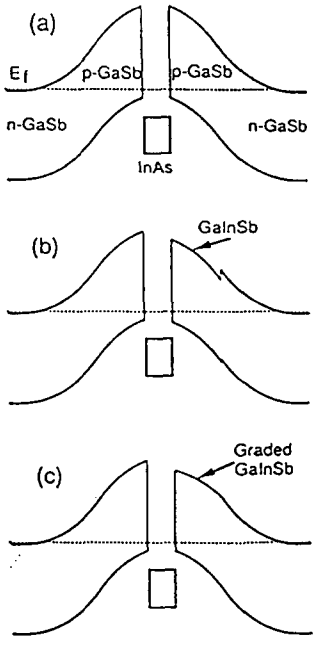

Fig. 25. Schematic energy-band diagrams of hot-electron transistors [146]: (a) a HET with GaSb collector; (b) a HET with GaInSb layer at the collector edge; (c) a HET with $Ga_{1-x}In_xSb$ graded layer at the collector edge.

rather than scattering in the base, although Auger actions may contribute to the scattering of energetic electrons in the InAs because of the small band gap. In further work InAs base widths as low as 30 Å were fabricated for a symmetric transistor (GaSb emitter and collector) but the current gains were low [147].

In another hot electron study n-AlSb was used as the emitter, and the base and collector were pn-InAs [148]. The emitter efficiency and current transfer ratio were small. Enough has been done to suggest that there is little point in further hot electron transistor studies when FETs of InAs are more promising. Finally it should be remarked that homojunction bipolar npn and pnp InAs transistors have received little attention, and these may also have more to offer than InAs hot electron transistors.

4. Quantum well structures and superlattices

Quantum wells involving InAs are of interest because of the large barriers that exist to GaSb or (AlGa)Sb, see Fig. 1(b). An example is shown in Fig. 27 where the separation of electrons and holes associated with the broken gap heterojunction of GaSb–InAs results in electron densities in the well of about 10^{12} cm^{-2} [149]. Electron storage in InAs wells bounded by $AlAs_{0.16}Sb_{0.84}$ has been studied and found to have a decay time constant of 50 s at 77 K [150]. The ΔE_c

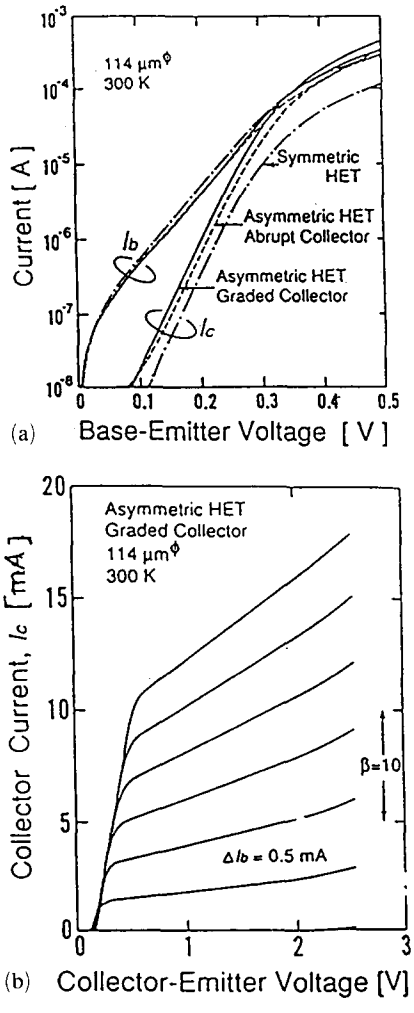

Fig. 26. Hot electron transistor characteristics [147]: (a) Gummel plots of the three types of HET structure; (b) common-emitter I–V characteristics of the asymmetrical HET with a graded $Ga_{0.9}In_{0.1}Sb$ collector. The emitter contact was alloyed Au–Ge.

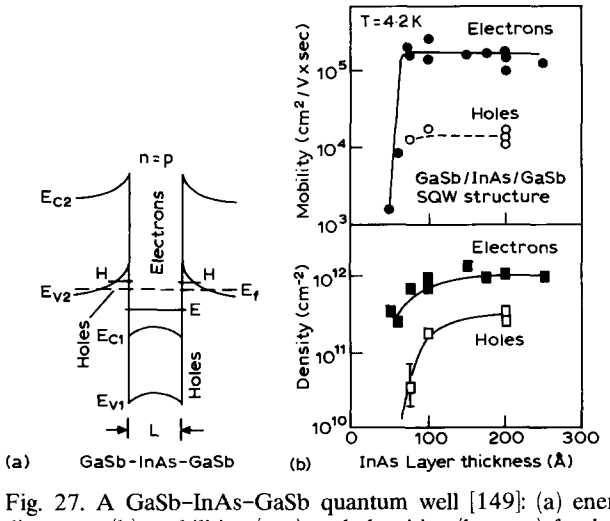

Fig. 27. A GaSb–InAs–GaSb quantum well [149]: (a) energy diagrams; (b) mobilities (top) and densities (bottom) for both electrons (in InAs) and holes (in GaSb) as a function of InAs well width at 4.2 K.

barrier height was considered to be about 1.06 eV and ΔE_v about 0.27 eV.

In a study of an AlSb–InAs quantum well, the total electron concentration was accounted for in terms of a contribution from the surface, and a combined bulk and interface contribution [151] as in Fig. 28. The surface contribution comes from a donor at the AlSb top surface so the width of the barrier determines the size of the term. InAs itself is noted for a high surface conductivity resulting from an accumulation of electrons [26–33, 152].

Short period superlattices of InAs–GaAs result in modification of barrier heights with E_v(InAs)–E_v (GaAs) becoming 0.55 eV [153] in contrast to about 0.19 eV shown in Fig. 1(b). The band offsets expected in an $Al_{0.8}Ga_{0.2}As_{0.14}Sb_{0.86}$–InAs superlattice are shown in Fig. 29. It is seen that the 1e and 2e electron states are well separated in the InAs [154]. The inclusion of interface strain can change the character of the band offsets from slightly to strongly staggered.

One of the reasons for the study of strained layer superlattices such as $InAs_{1-x}Sb_x$–InAs is to attempt to make use of the 0.15 eV energy band minimum shown in Fig. 20 at $x = 0.65$ [126] for infrared detectors out to about 8 μm wavelength. Photoluminescence of $InAs_{1-x}Sb_x$ on InAs has been seen to 8 μm [155] in studies of MBE growth parameters. One of the problems with such superlattices is the photon absorption,

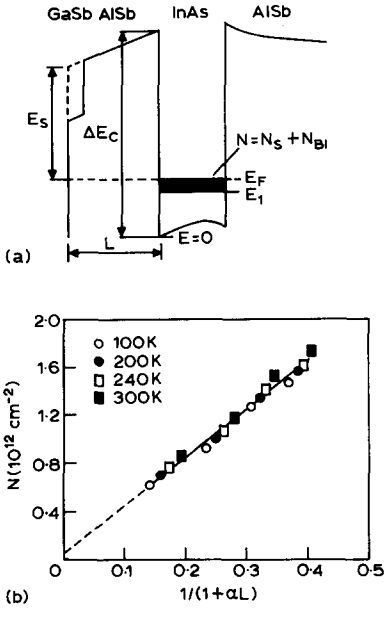

Fig. 28. An InAs–AlSb quantum well [151]. (a) Schematic energy band diagram of the InAs–AlSb quantum well. The sheet concentration N is the sum of a contribution from the surface N_s, and a combined bulk and interface contribution N_{BI}; (b) total concentration for wells of different thickness. The line may be interpreted to show the presence of the surface contribution from the AlSb with an activation energy 0.85 eV.

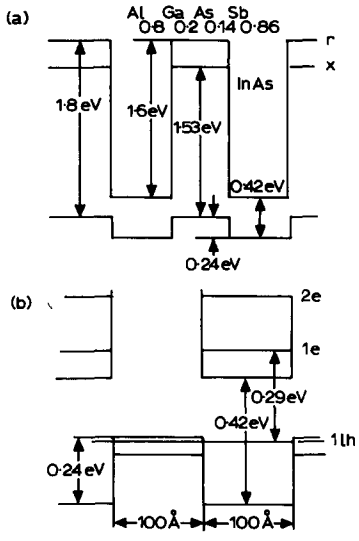

Fig. 29. An $Al_{0.8}Ga_{0.2}As_{0.14}As_{0.86}$–InAs superlattice [154]: (a) predicted band offsets; (b) energy levels for a 100 Å InAs well width.

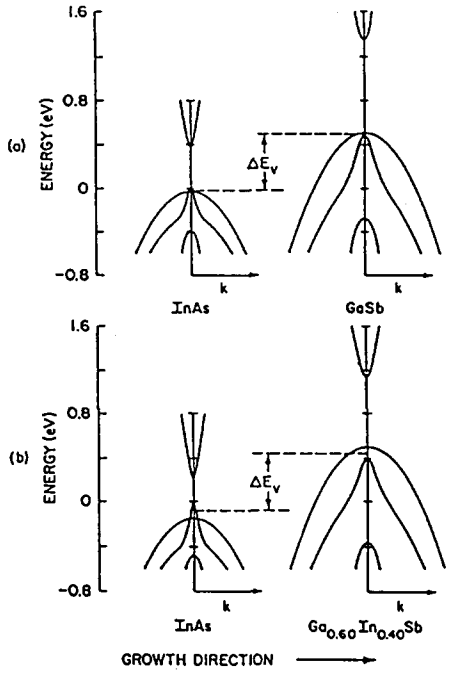

Fig. 30. Effects of lattice-mismatch-induced strain on the bulk electronic band structure of epitaxial growth InAs and $Ga_{1-x}In_xSb$ near the center of the Brillouin zone [158] for a (111) growth axis superlattice. Bulk energy dispersions are shown for a wave vector parallel to the superlattice (111) growth axis. The InAs($Ga_{1-x}In_xSb$) layers are under biaxial tensile (compressive) stress because of the lattice mismatch. The prescription for lining up the bulk band structures at the heterointerface is also indicated. Panel (a): strain configuration for $x = 0$ (lattice mismatch of 0.65%). Panel (b): strain configuration for $x = 0.40$ (lattice mismatch of 3.1%).

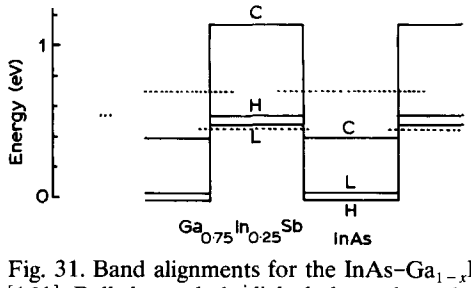

Fig. 31. Band alignments for the InAs–$Ga_{1-x}In_xSb$ superlattice [161]. Bulk heavy-hole, light-hole, and conduction-band edges are indicated by H, L, and C, respectively. Localization of electrons in the InAs layers and holes in the $Ga_{1-x}In_xSb$ is indicated by the dashed line superlattice energy levels.

with the light incident to the plane of the superlattice, is not efficient. Attempts have been made to improve absorption by the application of light parallel to the junction plane but the problems are severe [157]. $InAs_{1-x}Bi_x$ has been suggested as an alternative to $InAs_{1-x}Sb_x$ for long wavelength detectors but the work is too preliminary to discuss here. Neither need InSb be discussed here since an extensive literature already exists on this material.

It may be mentioned in passing that in InAs–GaSb superlattices, the application of light creates a small photovoltage of the order of 50 mV (with a decay time of hundreds of nanoseconds) which arises from the spacial separation of the electrons and holes [156, 157]. No device use has been reported for this effect.

There have been extensive studies of $Ga_{1-x}In_xSb$–InAs strained layer superlattices [158–167]. It has been suggested that for $x = 0.4$ such superlattices may have promising electro-optical properties for infrared detection. Some effects of strain on the band structure of InAs, GaSb, and $Ga_{0.60}In_{0.40}Sb$ are shown in Fig. 30 [158]. For a broken gap alignment as shown in Fig. 31 for InAs–$Ga_{0.75}In_{0.25}Sb$ with periods less than 75 Å it has been found that energy gaps corresponding to wavelengths greater than 8 μm can be obtained. An absorption coefficient of approximately 2000 cm^{-1} at 10 μm has been measured in a superlattice with an energy gap corresponding to 11.4 μm wavelength [161].

Calculations have been made of far-infrared absorption in InAs–AlGaSb quantum wells [167]. Intersubband absorptions in multiple quantum well structures normally have selection rules that only allow absorption of electromagnetic radiation when the incident polarization is parallel to the growth (confinement) direction. However in the InAs–AlGaSb structure the rules may be less restrictive and improved absorption may be obtained. Valence band splitting in Ga(AsSb) on InAs has been discussed by Mani *et al.* [168].

InAs–GaAs strained layer superlattices have been grown on GaAs (100), (111), (311) and (711) substrates in a search for quantum pyramid-type structures [169]. $(InAs)_m$ $(GaAs)_m$ short period superlattices have been grown on InP [170]. Structural stability of ultrathin InAs–GaAs quantum wells has been studied [171] and appears satisfactory. (AlGa)Sb tilted superlattices have been combined with InAs to form quantum wells with corrugated barriers in an exploration of quantum wire structure possibilities [172].

InAs or InAs–AlSb may be used as a superconducting channel weak link between Nb electrodes at 1.4 K [173, 174]. The use of undoped InAs wells with electrons obtained from the doping in the AlSb confining layer results in high electron mobilities and large superconducting coherence lengths in the channel. This gives a large (lineal) channel supercurrent of 32 mA mm^{-1} at 1.4 K for a channel length of 0.6 μm. This increases by four times when a magnetic field is applied and represents an areal current density of almost 10^6 A cm^{-2} and therefore very promising behavior.

A wide range of tunnel actions from InAs through barriers such as AlSb and AlGaSb has been seen [175–180] including peak-to-valley ratios between six and 60 at 77 K. InAs junctions have also been proposed as low-voltage backward diodes for small signal circuits. Although there are circuits where two-terminal negative resistance devices may find use as oscillators or bistable elements the applications are few, and the interest is more in the physics of the situation than in device uses.

5. Conclusions

InAs and related ternaries and quaternaries of closely similar lattice constant, exhibit interesting optical properties for lasers and detectors in the range up to 4 μm wavelength. In conjunction with $InAs_{1-x}Sb_x$ the range is extended to about 10 μm.

The high electron mobility (20 000 cm^2 V^{-1} s^{-1} at room temperature and 60 000 cm^2 V^{-1} s^{-1} at 77 K) offers the potential of high frequency field effect transistors. The low bandgap (0.36 eV) results in a low electric field strength for avalanche that limits junction performance. Interactions with magnetic fields are strong and InAs can be the basis of sensitive magnetic field detectors.

InAs may be used as a substrate for many lattice-matched quaternaries of (Al,Ga,In)(As,Sb) the properties of which remain largely unexplored. Multiple quantum wells and superlattices involving InAs and strained layer conditions can result in negative resistance tunnel devices of high peak-to-valley ratios.

Acknowledgments

This work has been supported in part by NSF Grant ECS 8915034. A. Y. Polyakov was on a leave of absence at Carnegie Mellon University from the Institute of Rare Metals, Moscow, Russia during this work. Discussions with Prof. A. Z. Li of Shanghai Institute of Metallurgy, Academia Sinica are also gratefully acknowledged.

References

1 J. A. Lott, L. R. Dawson, E. D. Jones, I. J. Fritz, J. S. Nelson and S. R. Kurtz, Molecular beam epitaxy and characterization of $Al_xGa_{1-x}As_ySb_{1-y}$ $(0.0 \leq x \leq 1.0)$ lattice matched to InAs substrates, *J. Electro. Mat., 19* (9) (1990) 989.
2 O. Madelung, *Physics of III–V Compounds*, Wiley, New York, 1964.
3 N. N. Sirota, Heats of formation and temperature and heats of fusion of compounds $A^{III}B^{V}$ in R. K. Willardson and A. C. Beer (eds.), *Semiconductors and Semimetals, Vol. 4, Physics of III–V Compounds*, Academic Press, New York, 1968, Chapter 2, p. 35.
4 M. Cardona, Optical absorption above the fundamental edge, in R. K. Willardson and A. C. Beer (eds.), *Semiconductors and Semimetals, Vol. 3*, Academic Press, New York, Chapter 5, p. 125.
5 J. C. Phillips, *Bonds and Bands in Semiconductors*, Academic Press, New York, 1973.
6 N. V. Zotova, G. Garyagdyev and D. N. Nasledov, Investigation of the structure of the allowed-band edges of n-type InAs by the optical absorption method, *Sov. Phys. Semicond., 8* (5) (1974) 593.
7 Yu. B. Ermolovich and A. F. Kravchuk, Influence of higher bands on the transport properties on n-type indium arsenide, *Sov. Phys. Semicond., 12* (5) (1978) 566.
8 I. Ya Nikiforov and A. T. Kozakov, Distribution of p-electrons in the valence bands of semi-conductors InAs and InSb, *Sov. Phy. Semicond., 8* (7) (1975) 901.
9 J. P. McCarthy, Preparation and properties of epitaxial InAs, *Solid-State Electronics, 10* (1967) 649.
10 L. E. Vorob'ev, Intraband luminescence and absorption of infrared radiation in n-type InAs subjected to strong electric fields, *Sov. Phys. Semicond., 8* (7) (1975) 839.
11 J. D. Wiley, Mobility of holes in III–V compounds, in R. K. Willardson and A. C. Beer (eds.), in *Semiconductors and Semimetals, Vol. 10, Transport Phenomena*, Academic Press, New York, Chapter 2, p. 91.
12 L. A. Kazakova, Yu, K. Shalabutov and Yu. I. Ukhanov, Optical investigation of p-type indium arsenide, *Sov. Phys. Semicond., 13* (2) (1979) 141.
13 V. N. Morozov and V. G. Chernov, Electrical properties and the mechanism of electron scattering in Te-doped InAs crystals in a wide temperature range, *Sov. Phys. Semicond., 14* (7) (1980) 863.
14 V. V. Karataev, M. G. Mil'vidskii, N. S. Rytova and V. I. Fistul, Compensation in n-type InAs, *Sov. Phys. Semicond., 11* (9) (1977) 1009.
15 L. E. Vorob'ev and F. I. Osokin, Intraband absorption of light in n-type InAs containing electric-field-heated electrons, *Sov. Phys. Semicond., 13* (8) (1979) 873.

16 L. A. Balagurov and É. M. Omel'yanovskii, Equilibrium conductivity and photoconductivity of strongly compensated InAs, *Sov. Phys. Semicond.*, *14* (10) (1980) 1158.
17 V. M. Glazov and V. A. Nagiev, Impurity-concentration dependence of the number of carriers in indium arsenide doped with donors and acceptors and the relationship of this dependence to the solubility limit, *Sov. Phys. Semicond.*, *8* (1) (1974) 82.
18 L. A. Balagurov, É. M. Omel'yanovskii and V. I. Fistul, Energy positions of deep levels in high-resistivity InAs:Cr, *Sov. Phys. Semicond.*, *11* (2) (1977) 1404.
19 M. P. Mikhailova, A. V. Pentsov and S. V. Siobodchikov, Photoconductivity of compensated n-type InAs, *Sov. Phys. Semicond.*, *9* (7) (1976) 817.
20 A. Plitnikas, A. Krotkus and Z. Dobrovol'skis, Current-voltage characterization of compensated indium arsenide in strong electric fields, *Sov. Phys. Semicond.*, *16* (6) (1982) 622.
21 E. I. Georgitsé, I. T. Postolaki, V. A. Smirnov and P. G. Untila, Photoluminescence of p-type InAs:Mn, *Sov. Phys. Semicond.*, *23* (4) (1989) 469.
22 N. G. Kolin, V. B. Osvenskii, N. S. Rytova and E. S. Yurova, Properties of nuclear-transmutation-doped indium arsenide, *Sov. Phys. Semicond.*, *20* (5) (1986) 519.
23 I. A. Fomin, L. V. Lebedeva and N. M. Annenko, Investigation of deep levels in InAs by measurement of the capacitance of metal-insulator-semiconductor structures, *Sov. Phys. Semicond.*, *18* (4) (1984) 457.
24 E. H. Putley, *The Hall Effect and Related Phenomena*, Butterworths, London, 1960.
25 Ya Agaev, M. Meredov, M. P. Mikhailova and S. V. Slobidchikov, Influence of a magnetic field on the photosensitivity spectrum of InAs p-n junctions, *Sov. Phys. Semicond.*, *13* (2) (1979) 231.
26 H. H. Wieder, Transport coefficients of InAs epilayers, *Appl. Phys. Lett.*, *25* (4) (1974) 206.
27 H. A. Washburn, J. R. Sites and H. H. Weider, Electronic profile of n-InAs on semi-insulating GaAs, *J. Appl. Phys.*, *50* (7) (1979) 48.
28 D. C. Tsui, Electron-tunneling studies of a quantized surface accumulation layer, *Phys. Rev. B*, *4* (12) (1971) 4438.
29 D. C. Tsui, Electron tunneling and capacitance studies of a quantized surface accumulation layer, *Phys. Rev. B*, *8* (6) (1973) 265.
30 D. C. Tsui, Landau-level spectra of conduction electrons at an InAs surface, *Phys. Rev. B*, *12* (12) (1975) 5739.
31 E. Yamaguchi, Theory of defect scattering in two-dimensional multisubband electronic systems on III–V compound semiconductors, *J. Appl. Phys.*, *56* (6) (1984) 1722.
32 E. Yamaguchi, Electron subbands and transport properties in inversion layers of InAs and InP, *Phys. Rev. B*, *32* (8) (1985) 5280.
33 Y. Chen, J. C. Hermanson and G. J. Lapeyre, Coupled plasmon and phonon in the accumulation layer of InAs (110) cleaved surfaces, *Phys. Rev. B*, *39* (17) (1988) 12682.
34 H. Sakaki, L. L. Chang, G. A. Sai-Halasz, C. A. Chang and L. Esaki, Two-dimensional electronic structure in InAs–GaAs superlattices, *Solid State Commun.*, *26* (1978) 589.
35 G. W. Gobeli and F. G. Allen, Photoelectric threshold and work function, in R. K. Willardson and A. C. Beer (eds.), *Semiconductors and Semimetals, Vol. 2, Physics of III–V Compounds*, Academic Press, New York, 1966.
36 B. O. Seraphin and H. E. Bennett, Optical constants, in R. K. Willardson and A. C. Beer (eds.), *Semiconductors and Semimetals, Vol. 3*, Academic Press, New York, 1967, Chapter 12.
37 W. G. Spitzer, Multiphonon lattice absorption, in R. K. Willardson and A. C. Beer (eds.), *Semiconductors and Semimetals, Vol. 2, Physics of III–V Compounds*, Academic Press, New York, 1966, Chapter 2, p. 17.
38 M. I. Guseva, N. V. Zotova, A. V. Koval and D. N. Nasledov, Radiative recombination in indium arsenide implantation-doped with group IV elements, *Sov. Phys. Semicond.*, *9* (5) (1975) 591.
39 É. Adomaitis, Z. Dobrovol'skis and A. Krotkus, Picosecond photoconductivity of indium arsenide, *Sov. Phys. Semicond.*, *18* (8) (1984) 889.
40 M. P. Mikhailova, S. V. Slobodchikov, A. V. Pentsov and M. Khamrokulov, Oscillations of the photoconductivity and photomagnetic effect in n-type InAs, *Sov. Phys. Semicond.*, *10* (1) (1976) 115.
41 S. I. Novikova, Thermal Expansion, in R. K. Willardson and A. C. Beer (eds.), *Semiconductors and Semimetals, Vol. 2, Physics of III–V Compounds*, Academic Press, New York, 1966, Chapter 2, p. 33.
42 H. Terao, Y. Togasaki and Y. Sakai, Electrical and photoelectric properties of InAs junctions, *Electr. Eng. Jpn.*, *92* (2) (1974).
43 H. Terao, T. Ito and Y. Sakai, Interface properties of InAs–MIS structures and their application to FET, *Electr. Eng. Jpn.*, *94* (2) (1974).
44 A. Katz, S. N. G. Chu, B. E. Weir, W. Savin, D. W. Harris, W. C. Dautremont-Smith, T. Tanbun-Ek and R. A. Logan, Electrical and structural properties of Pt/Ti/p^+ -InAs ohmic contacts, *J. Vac. Sci. Technol.*, *B8* (5) (1990) 1125.
45 N. P. Esina, N. V. Zotova, S. A. Karandashev and G. M. Filaretova, Metal-semiconductor structures based on p-type InAs, *Sov. Phys. Semicond.*, *17* (6) (1983) 624.
46 S. L. Wright, R. F. Marks, S. Tiwari, T. N. Jackson and H. Baratte, In-situ contacts to GaAs based on InAs, *Appl. Phys. Lett.*, *49* (22) (1986) 1545.
47 H.-J. Kim, M. Murakami, S. L. Wright, M. Norcott, W. H. Price and D. La Tulipe, Thermally stable ohmic contacts to n-type GaAs. VIII. Sputter-deposited InAs contacts, *J. Appl. Phys.*, *68* (5) (1990) 2475.
48 Yu. G. Malinin, S. V. Slobodchikov and G. M. Filaretova, Spectral photosensitivity of Au-p-InAs Schottky diodes, *Sov. Phys. Semicond.*, *20* (5) (1986) 569.
49 Yu. G. Malinin, S. V. Slobodchikov, G. M. Filaretova and V. M. Fetisova, Influence of a magnetic field on the photoelectric effect in p-type InAs Schottky diodes, *Sov. Phys. Semicond.*, *19* (6) (1985) 686.
50 R. Veresegyházy, B. Pécz, and I. Mojzes, The influence of a gold layer on the thermal decomposition of InAs, *Phys. Status. Solidi (a)* *94* (1986) K11.
51 M. Yamaguchi, A. Yamamoto, H. Sugiura and C. Uemura, Thermal oxidation of InAs and characterization of the oxide film, *Thin Solid Films*, *92* (1982) 361.
52 H.-U. Bauer, L. Koenders and W. Mönch, Oxidation of InAs (110) and correlated changes of electronic surface properties, *J. Vac. Sci. Technol.*, *B4* (4) (1986) 1095.
53 J. N. Walpole, and K. W. Nill, Capacitance-voltage characterization of metal barriers on pPbTe and pInAs: effects of the inversion layer, *J. Appl. Phys.*, *42* (1971) 5609.
54 G. I. Kol'tsov and Yu. V. Krutenyuk, Tunneling and surface states in a contact between Au and p-type InAs, *Sov. Phys. Semicond.*, *23* (11) (1989) 1229.
55 H. Khald, H. Main and A. Joullie, Shallow diffusion of zinc into InAs and InAsSb, *J. Appl. Phys.*, *64* (9) (1988) 4768.

56 I. I. Zasavitskii, Radiation emitted from semiconductor lasers in strong magnetic fields and under high hydrostatic pressures, in *Optical Properties of Semiconductors, Vol. 76*, Consultant Bureau, New York, London.

57 A. G. Chynoweth, Charge multiplication phenomena, in R. K. Willardson and A. C. Beer (eds.), *Semiconductors and Semimetals, Vol. 4 Physics of III–V Compounds*, Academic Press, New York, 1968, Chapter 4, p. 263.

58 M. P. Mikhailova, N. N. Smirnova and S. V. Slobodchikov, Carrier multiplication in InAs and InGaAs p-n junctions and their ionization coefficients, *Sov. Phys. Semicond., 10* (5) (1976) 509.

59 D. L. Kendall, Diffusion, in R. K. Willardson and A. C. Beer (eds.), *Semiconductors and Semimetals, Vol. 4, Physics of III–V Compounds*, Academic Press, New York, 1968, Chapter 3, p. 163.

60 G. Bauer and F. Kuchar, Avalanche breakdown in n-type InAs at 77 K, *Phys. Lett., 30A* (7) (1969) 399; Impact ionization in heavily doped nInAs and nInSb, *Phys. Status Solidi, (a) 13* (1972) 169.

61 M. C. Steele and S. Tosima, Electron-hole scattering in solids exhibiting band-gap impact ionization, *Japan. J. Appl. Phys., 2* (7) (1963) 381.

62 P. J. McNally, Ion implantation in InAs and InSb, in F. H. Eisen and L. T. Chadderton (eds.), Gordon and Breach Science Publishers, London, 1971, p. 405.

63 I. P. Akimchenko, E. G. Panshina, O. V. Tikhonova, and E. A. Frimer, Photoelectric properties of indium arsenide doped by implantation of 350 keV S and Mg ions, *Sov. Phys. Semicond., 13* (11) (1979) 1292.

64 E. I. Georgitsé, I. T. Postolaki, V. A. Smirnov and P. G. Untila, Photoluminescence of p-type InAs:Mn, *Sov. Phys. Semicond., 23* (4) (1989) 469.

65 D. G. Andrianov, V. V. Karataev, G. V. Lazareva, Yu. B. Muravlev and A. S. Savel'ev, Interaction of carriers with localized magnetic moments in InSb:Mn and InAs:Mn, *Sov. Phys. Semicond., 11* (1977) 738.

66 N. N. Gerasimenko, A. M. Myasnikov, A. A. Nesterov, V. I. Obodnikov, L. N. Safronov and G. S. Khryashchev, Inversion of the type of conduction in p-type InAs films irradiated with argon ions, *Sov. Phys. Semicond., 22* (4) (1988) 470.

67 M. I. Guseva, N. V. Zotova, A. V. Koval' and D. N. Nasledov, Behavior of Group IV elements introduced into indium arsenide by ion implantation, *Sov. Phys. Semicond., 8* (1) (1974) 34; *Sov. Phys. Semicond., 9* (5) (1975) 591.

68 N. G. Kolin, V. B. Osvenskii, N. S. Rytova and E. S. Yurova, Electrical properties of indium arsenide irradiated with fast neutrons, *Sov. Phys. Semicond., 21* (3) (1987) 320.

69 R. J. Harrison and P. A. Houston, LPE growth and characterization of n-type InAs, *J. Crystal Growth, 78* (1986) 257.

70 R. D. Gruber, H. D. Drew, J. -I. Chyi, S. Kalem and H. Morkoc, Infrared photoluminescence of InAs epilayers grown on GaAs and Si substrates, *J. Appl. Phys., 65* (1989) 4079.

71 C. T. Foxon and B. A. Joyce, Surface processes controlling the growth of $Ga_xIn_{1-x}As$ and $Ga_xIn_{1-x}P$ alloy films by MBE, *J. Cryst. Growth, 44* (1978) 75.

72 J. D. Grange, E. H. C. Parker and R. M. King, Relationship of MBE growth parameters with the electrical properties of thin (100) InAs epilayers, *J. Appl. Phys., 12* (1979) 1601.

73 P. Goldfinger and M. Jeunehomme, in J. Waldman (ed.), *Advances in Mass Spectroscopy*, Pergamon, London, 1959, p. 534.

74 S. M. Newstead, R. A. A. Kubiak and E. H. C. Parker, On the practical applications of MBE surface phase diagrams, *J. Cryst. Growth, 81* (1987) 49.

75 R. A. A. Kubiak, E. H. C. Parker, S. Newstead and J. J. Harris, The morphology and electrical properties of heteroepitaxial InAs prepared by MBE, *Appl. Phys., A35*, (1984) 61.

76 M. Yano, K. Yoh, T. Iwaaki, Y. Iwai and M. Inoue, Structural stability of ultrathin InAs/GaAs quantum wells grown by migration enhanced epitaxy, *J. Cryst. Growth, 111* (1991) 397.

77 J. A. Lott, L. R. Dawson, E. D. Jones and J. F. Klem, Molecular beam epitaxy of $AlAs_{0.16}Sb_{0.84}$ and $Al_{0.8}Ga_{0.2}As_{0.14}Sb_{0.86}$ on InAs substrates, *Appl. Phys. Lett., 56* (13) (1990) 1242.

78 W. J. Schaffer, M. D. Lind, S. P. Kowalczyk and R. W. Grant, Nucleation and strain relaxation at the InAs/GaAs (100) heterojunction, *J. Vac. Sci. Technol., B1* (3) (1983) 688.

79 F. Houzay, C. Guille, J. M. Moison, P. Henoc and F. Barthe, First stages of the MBE growth of InAs on (001) GaAs, *J. Cryst. Growth, 81* (1987) 67.

80 S. Guha, K. C. Rajkumar and A. Madhukar, The nature and control of morphology and the formation of defects in InGaAs epilayers and InAs/GaAs superlattices grown via MBE on GaAs (100), *J. Cryst. Growth, 111* (1991) 434.

81 S. Subbanna, J. Gaines, G. Tuttle, H. Kroemer, S. Chalmers and J. H. English, Reflection high-energy electron diffraction oscillations during molecular-beam epitaxy growth of gallium antimonide, aluminum antimonide and indium arsenide, *J. Vac. Sci. Technol., B7* (2) (1989) 289.

82 H. Yamaguchi and Y. Horikoshi, Replacement of Group-III atoms on the growing surface during migration-enhanced epitaxy, *J. Appl. Phys., 68* (4) (1990) 1610.

83 O. Brandt, L. Tapfer, G. Scamarcio, R. Cingolani and K. Ploog, Growth processes and relaxation mechanisms in the molecular beam epitaxy of InAs/GaAs heterostructures, *J. Cryst. Growth, 111* (1991) 383.

84 P. A. Thiry, J. L. Longueville, J. J. Pireaux, R. Caudano, H. Munekata and M. Liehr, Investigation of InAs and GaSb by high-resolution electron energy-loss spectroscopy, *J. Vac. Sci. Technol. A5* (4) (1988) 603.

85 K. Kudo, J. Lee, K. Tanaka, Y. Makita and A. Yamada, Fabrication and characterization of MBE grown InAs/GaAs strained-layer superlattices on variously orientated substrates, *J. Cryst. Growth, 111* (1991) 402.

86 M. Y. Yen, B. F. Levine, C. G. Bethea, K. K. Choi and A. Y. Cho, Molecular beam epitaxy growth and optical properties of $InAs_{1-x}Sb_x$ in 8–12 μm wavelength range, *Appl. Phys. Lett., 50* (14) (1987) 927.

87 M. Y. Yen, R. People, K. W. Wecht and A. Y. Cho, Long-wavelength photoluminescence of $InAs_{1-x}Sb_x$ $(0 < x < 1)$ grown by molecular beam epitaxy on (100) InAs, *Appl. Phys. Lett., 52* (6) (1988) 489.

88 O. Mizuno, H. Watanabe and D. Shinoda, Vapor growth of InAs, *Japan. J. Appl. Phys., 14* (2) (1975) 184.

89 S. F. Fang, K. Matsushita and T. Hariu, Plasma-assisted epitaxial growth of InAs, *Appl. Phys. Lett., 54* (14) (1989) 1338.

90 Z. M. Fang. K. Y. Ma, R. N. Cohen and G. B. Stringfellow, Effect of growth temperature on photoluminescence of InAs grown by organometallic vapor phase epitaxy, *Appl. Phys. Lett., 59* (12) (1991) 1447.

91 M. Koch, O. Acher, F. Omnes, M. Defour, M. Razeghi and B. Drévillon, In-situ investigation of InAs metalorganic chemical vapor deposition growth using reflectance anisotropy, *J. Appl. Phys., 68* (7) (1990) 3364.

92 R. W. Martin, M. Lakrimi, S. K. Haywood, R. J. Nicholas, N. J. Mason, and P. J. Walker, Semimetallic behavior in GaSb–InAs heterojunctions, *Proc. Int. Conf. on the Appli-*

cation of High Magnetic Fields in Semiconductor Physics, Würzburg, 1990, Springer-Verlag, Germany.
93 S. K. Haywood, R. W. Martin, N. J. Mason, R. J. Nicholas and P. J. Walker, GaSb-InAs heterojunctions grown by MOVPE, *J. Cryst. Growth, 107* (1991) 422.
94 M. Lakrimi, R. W. Martin, N. J. Mason, R. J. Nicholas and P. J. Walker, GaSb-InAs heterojunctions grown by MOVPE: effect of gas switching sequences on interface quality, *J. Cryst. Growth, 110* (1991) 677.
95 T. H. Glisson, J. R. Hauser, M. A. Littlejohn and C. K. Williams, Energy bandgap and lattice contours of III-V quaternary alloys, *J. Electron. Mat.*, 7(1) (1978) 1.
96 C. K. Williams, T. H. Glisson, J. R. Hauser and M. A. Littlejohn, Energy bandgap and lattice constant contours of III-V quaternary alloys of the form $A_xB_yC_zD$ or $AB_xC_yD_z$, *J. Electron. Mat.*, 7(5) (1978) 639.
97 S. Adachi, Bandgaps and refractive indices of AlGaAsSb, GaInAsSb, and InPAsSb: key properties for a variety of the 2-4 μm optoelectronic device applications, *J. Appl. Phys., 61* (10) (1987) 4869.
98 A. G. Milnes and D. L. Feucht, *Heterojunctions and Metal-Semiconductor Junctions*, Academic Press, New York, 1972.
99 G. J. Gualtieri, R. G. Nuzzo, R. J. Malik, J. F. Walker, L. C. Feldman, W. A. Sunder and G. P. Schwartz, Summary abstract: valance-band discontinuities in (100) GaSb-AlSb and GaSb-InAs heterojunctions, *J. Vac. Sci. Technol., B5* (4) (1987) 1284.
100 S. P. Kowalczyk, W. J. Schaffer, E. A. Kraut and R. W. Grant, Determination of the InAs-GaAs (100) heterojunction band discontinuities by X-ray Photoelectron Spectroscopy (XPS), *J. Vac. Sci. Technol., 20* (3) (1982) 705.
101 H. Kroemer, Heterostructure devices: a device physicist looks at interfaces, *Surf. Sci., 132* (1983) 543.
102 W. Both, A. Bochkarev, A. Drakin and B. Sverdlov, Thermal resistivity of quaternary solid solutions InGaSbAs and GaAlSbAs lattice-matched to GaSb, *Electron. Lett., 26* (7) (1990) 418.
103 E. G. Bithell and W. M. Stobbs, Ternary semiconductor heterostructures: the choice of an appropriate compositional analysis technique, *J. Appl. Phys., 69* (4) (1991) 2149.
104 J. H. Kim, D. Yang, Y. -C. Chen and P. Bhattacharya, Growth and properties of $InAs_xSb_{1-x}$, $Al_yGa_{1-y}Sb$, and $InAs_xSb_{1-x}/Al_yGa_{1-y}Sb$ heterostructures, *6th Int. MBE Conf. Abstracts 1990. J. Crystal Growth, 111* (1991) 633.
105 M. D. Williams and T. H. Chiu, The effect of strain on the valence band structure of InAs (100), *J. Vac. Sci. Technol., B8* (4) (1990) 758.
106 H. Mani, A. Joullie, A. M. Joullie, B. Girault and C. Alibert, Band-gap and spin-orbit splitting of the lattice-matched GaAsSb-InAs system, *J. Appl. Phys., 61* (5) (1987) 2101.
107 P. Sheldon, M. M. Al-Jassim, K. M. Jones, J. P. Goral and B. G. Yacobi, Structural and electrical characterization of InAs grown on GaAs substrates by molecular beam epitaxy, *J. Vac. Sci. Technol., A7* (3) (1989) 770.
108 M. S. Bresler, O. B. Gusev, M. P. Mikhailova, V. V. Sherstnev, Yu, I. Yakovlev and I. N. Yassievich, Interface luminescence due to above-barrier reflection in an isotypic p-InAs-P-InAsPSb heterostructure, *Sov. Phys. Semicond., 25* (2) (1991) 181.
109 Zh. I. Alferov, M. Z. Zhingarev, V. I. Korol'kov, N. N. Mursakulov, L. D. Pramatarova and D. N. Tret'yakov, Electrical and photoelectric properties of $InAs-Al_yGa_{1-x}Sb$ heterojunctions, *Sov. Phys. Semicond., 12* (2) (1977) 180.
110 L. Schuermeyer, P. Cook, E. Martinez and J. Tantillo, Band-edge alignment in heterostructures, *Appl. Phys. Lett., 55* (18) (1989) 1877.
111 B. I. Sysoev, B. L. Agapov, N. N. Bezryadin, A. V. Budanov, T. V. Prokopova and S. V. Fetisova, Properties of an interface between InAs and a thin semi-insulating In_2S_3 film, *Sov. Phys. Semicond., 25* (4) (1991) 421.
112 T. -H. Shen, M. Elliot, R. H. Williams and D. Westwood, Effective barrier height, conduction-band offset, and the influence of p-type δ doping at heterojunction interfaces: the case of the InAs-GaAs interface, *Appl. Phys. Lett., 58* (8) (1991) 842.
113 A. C. Diebold, S. W. Steinhauser and R. P. Mariella, Jr., Use of Raman spectroscopy to characterize strain in III-V epilayers: application to InAs on GaAs (001) grown by molecular beam epitaxy, *J. Vac. Sci. Technol., B7* (2) (1989) 365.
114 G. Hollinger, D. Gallet, M. Gendry, C. Santinelli and P. Viktorovitch, Structural and chemical properties of InAs layers grown on InP (100) surfaces by arsenic stabilization, *J. Vac. Sci. Technol., B8* (4) (1990) 832.
115 V. V. Evstropov, N. M. Stus', N. N. Smirnova, G. M. Filaretova, L. M. Fedorov and V. G. Sidorov, Non-classical thermal injection current in InAsSbP-InAs p-n structures, *Sov. Phys. Semicond., 20* (4) (1986) 482.
116 B. A. Matveev, V. I. Petrov, N. M. Stus', G. N. Talalakin and A. V. Shabalin, Cathodoluminescence of graded-gap epitaxial InAsSbP-InAs structures, *Sov. Phys. Semicond., 22* (7) (1988) 788.
117 J. Singh, S. Dudley, B. Davies and K. K. Bajaj, Role of kinetics and thermodynamics in alloy clustering and surface quality in InAlAs grown by molecular beam epitaxy: consequences for optical and transport properties, *J. Appl. Phys., 60* (9) (1986) 3167.
118 A. G. Milnes, *Semiconductor Devices and Integrated Electronics*, Van Nostrand-Reinhold, New York, 1980, Chapter 13.
119 W. L. Eisenman (ed.), Utilization of infrared detectors, *SPIE Meeting Jan. 16-18, 1978, Los Angeles, CA*, SPIE, Bellingham, WA, 1978, SPIE Vol. 132.
120 W. L. Eisenman, J. D. Merriam and R. F. Potter, Operational characteristics of infrared photodetectors, in R. K. Willardson and A. C. Beer (eds.), *Semiconductors and Semimetals, Vol. 11, Infrared Detectors*, Academic Press, New York, Chapter 1, p. 1.
121 H. Levinstein and J. Mudar, Infrared detectors in remote sensing, *Proc. IEEE, 63* (1975) 6.
122 G. E. Stillman and C. M. Wolfe, Avalanche photodiodes in R. K. Willardson and A. C. Beer (eds.), *Semiconductors and Semimetals, Vol. 12, Infrared Detectors*, Academic Press, New York, Chapter 5, p. 291.
123 C. Hilsum and O. Simpson, The design of single crystal infrared photocells, *Proc. IEEE, 106 (B)* (1960) 398.
124 P. W. Kruse, L. D. McGlauchlin and R. B. McQuistan, *Elements of Infrared Technology: Generation Transmission and Detection*, Wiley, New York, 1962.
125 Z. Mohammed, F. Capasso, R. A. Logan, J. P. van der Ziel and A. L. Hutchinson, High-detectivity $InAs_{0.85}Sb_{0.15}$-InAs infrared (1.8-4.8 μm) detectors, *Electron. Lett., 22* (4) (1986) 215.
126 R. M. Biefeld, S. R. Kurtz, L. R. Dawson and G. C. Osbourn, The preparation and infrared properties of In (AsSb) strained-layer superlattices, *Crystal Properties Preparation, Vol. 21*, Trans. Tech. Publications, Switzerland, 1989, pp. 141-164.
127 S. R. Kurtz, R. M. Biefeld, L. R. Dawson, I. J. Fritz and T. E.

Zipperian, High photoconductivity gain in lateral InAsSb strained-layer superlattice infrared detectors, *Appl. Phys. Lett., 53*(20)(1988)1961.
128 S. R. Kurtz, L. R. Dawson, T. E. Zipperian and R. D. Whaley, Jr., High-detectivity ($>1\times10^{10}$cm$\sqrt{}$Hz/W), InAsSb strained-layer superlattice, photovoltaic infrared detector, *IEEE Electron Devices Lett., 11* (1)(1990)54.
129 K. C. Hass and D. J. Kirill, In(As,Sb) sawtooth doping superlattices for long wavelength infrared detection, *J. Appl. Phys., 68*(4)(1990)1923.
130 C. W. Wu and H. H. Lin, Two-dimensional simulation on the electric field spike of indium antimonide charge injection devices, *Solid St. Electron., 33*(9)(1990)1169.
131 I. Melngailis and R. H. Rediker, Properties of InAs lasers, *J. Appl. Phys., 37*(2)(1966)899.
132 M. A. C. S. Brown and P. Porteous, The technology and properties of epitaxial indium arsenide lasers, *J. Appl. Phys., 18*(1967)1527.
133 V. B. Buber, V. V. Nikitin and K. P. Fedoseev, Investigation of the time constants of an indium arsenide laser, in S. M. Ryvkin and Yu, V. Shmartsev (eds.), *Physics of p-n Junctions and Semiconductor Devices*, Consultants Bureau, New York-London, 1971.
134 S. J. Eglash and H. K. Choi, Efficient GaInAsSb-AlGaAsSb diode lasers emitting at 2.29 μm, *Appl. Phys. Lett., 57*(1990)1292.
135 H. K. Choi and S. J. Eglash, Room temperature CW operation at 2.2 μm of GaInAsSb-AlGaAsSb diode lasers grown by molecular beam epitaxy, *Appl. Phys. Lett., 59*(10)(1991) 1165-1166; High power multiple quantum well GaInAsSb-AlGaAsSb diode lasers emitting at 2.1 μm with low threshold current density, submitted for publication *Appl. Phys. Lett.* (1992).
136 Y. Horikoshi, Semiconductor lasers with wavelengths exceeding 2 μm, *Semiconduc. Semimet. C, 22*(1985)93.
137 A. Cappy, B. Carnez, R. Fauquembergues, G. Salmer and E. Constant, Comparative potential performance of Si, GaAs, GaInAs, InAs submicrometer-gate FETs, *IEEE Trans. Electron Devices, ED-27*(1980)2158.
138 T. P. Brody and H. E. Kunig, A high-gain InAs thin-film transistor, *Appl. Phys. Lett., 9*(7)(1966)259.
139 H. E. Kunig, Analysis of an InAs thin film transistor, *Solid St. Electron. 11*,(1968)335.
140 K. Yoh, T. Moriuchi and M. Inoue, An InAs channel heterojunction field-effect transistor with high transconductance, *IEEE Electron Devices Lett., 11* (11)(1990)526.
141 D. Frank, D. C. LaTulipe Jr. and H. Munekata, Novel InAs-(Al, Ga)Sb FET with direct gate-to-channel contact, *IEEE Electron Devices Lett., 12* (5)(1991p 210.
142 K. F. Longenbach, R. Beresford and W. I. Wang, A complementary heterostructure field effect transistor technology based on InAs-AlSb-GaSb, *IEEE Trans. Electron Devices, 37*(10)(1990)2265.
143 K. Yoh, K. Kiyomi, H. Taniguchi, M. Yaho and M. Inoue, A p-channel GaSb heterojunction field effect transistor based on a vertically integrated complementary circuit structure, in G. B. Stringfellow (ed.), *GaAs and Related Compounds, Inst. of Phys. Conf. Ser., 120*, Institute of Physics, Bristol, Philadelphia and New York, 1991, p. 173.
144 A. G. Milnes and A. Y. Polyakov, Gallium antimonide device related properties, *Solid St. Electron.*, in press.
145 R. K. Reich and D. K. Ferry, A two-dimensional simulation of a cooled, submicrometer indium arsenide Schottky-gate FET, *IEEE Trans. Electron Devices, ED-27*(1980)6.
146 K. Taira, F. Nakamura, K. Funato and H. Kawai, Room-temperature operation of GaSb-InAs hot electron transistors grown by MOCVD, *Inst. Phys. Conf. Ser. No. 112, Int. Symp. GaAs and Related Compounds, Jersey 1990*, Chapter 7, p. 489.
147 K. Taira, K. Funato, F. Nakamura and H. Kawai, InAs quantum-well-base InAs-GaSb Hot-electron transistors, *J. Appl. Phys., 69 (8)* (1991)4454.
148 A. S. Vengurlekar, F. Capasso and T. H. Chiu, Impact ionization in the base of a hot-electron AlSb-InAs bipolar transistor, *Appl. Phys, Lett., 57*(17)(1990)1772.
149 G. Bastard and J. A. Brum, Electronic states in semiconductor heterostructures, *IEEE J. Quantum Electron., QE 22*(9)(1986)1625.
150 J. A. Lott, L. R. Dawson, H. T. Weaver, T. W. Zipperian and R. B. Caldwell, Investigation of charge storage in InAs-AlAsSb quantum well capacitors, *Appl. Phys. Lett., 55*(11)(1989)1118.
151 C. Nguyen, B. Brar, H. Kroemer and J. H. English, Surface donor contribution to electron sheet concentrations in not-intentionally doped InAs-AlSb quantum wells, *Appl. Phys. Lett., 60*(15)(1992)1854.
152 L. A. Balagurov, Y. E. Lozovik and É. M. Omel'yanovskii, Anderson localization in a two-dimensional accumulation layer on the surface of InAs, *Sov. Phys. Semicond., 14* (3)(1980)352.
153 Y. Hashimoto, K. Hirakawa, K. Harada and T. Ikoma, Strain induced change in band off-sets at pseudomorphically grown InAs-GaAs heterointerfaces characterized by X-ray photo-electron spectroscopy, *J. Cryst. Growth, 111* (1991)393.
154 J. S. Nelson, S. R. Kurtz, L. R. Dawson and J. A. Lott, Demonstration of the effects of interface strain on band offsets in lattice-matched III-V semiconductor superlattices, *Appl. Phys. Lett., 57*(6)(1990)578.
155 M. Y. Yen, R. People, K. W. Wecht and A. Y. Cho, Long-wavelength photoluminescence of $InAs_{1-x}Sb_x$ $(0<x<1)$ grown by molecular beam epitaxy on (100) InAs, *Appl. Phys. Lett., 52*(6)(1988)489.
156 L. R. Dawson, personal communication.
157 J. Bleuse, P. Voisin, M. Voos, H. Munekata, L. L. Chang and L. Esaki, Investigations of the quantum photovoltaic effect in InAs-GaSb semiconductor superlattices, *Appl. Phys. Lett., 52*(6)(1988)462.
158 C. Mailhoit and D. L. Smith, Electronic structure of (001) and (111) growth axis InAs-$Ga_{1-x}In_xSb$ strained-layer superlattices, *J. Vac. Sci. Technol., B5*(4)(1987)1268.
159 D. H. Chow, R. H. Miles, J. R. Söderström and T. C. McGill, Growth and characterization of InAs-$Ga_{1-x}In_xSb$ strained-layer superlattices, *Appl. Phys. Lett., 56* (15)(1990)1418.
160 R. Fashe, J. T. Zborowski, T. D. Golding, H. D. Shih, P. C. Chow, K. Matsuichi, B. C. Covington, A. Chi, J. Zheng, and H. F. Schaake, MBE growth and characterization of $In_xGa_{1-x}Sb$-InAs strained layer superlattices, *6th Int. MBE Conf., J. Crystal Growth, 111*(1991)677.
161 R. H. Miles, D. H. Chow, J. N. Schulman, T. C. McGill, Infrared optical characterization of InAs-$Ga_{1-x}In_xSb$ superlattices, *Appl. Phys. Lett., 57*(8)(1990)801.
162 D. W. Chow, R. H. Miles, J. R. Söderstrom and T. C. McGill, InAs-$Ga_{1-x}In_xSb$ strained-layer superlattices grown by molecular beam epitaxy, *J. Vac. Sci. Technol., B8* (4)(1990)710.
163 I. Sela, I. H. Campbell, B. K. Laurich, D. L. Smith, L. A. Samoska, C. R. Bolognesi, A. C. Gossard and H. Kroemer, Raman scattering study of InAs-GaInSb strained layer superlattices, *J. Appl. Phys., 70*(10)(1991)5608.

164 I. H. Campbell, I. Sela, B. K. Laurich, D. L. Smith, C. R. Bolognesi, L. A. Samoska, A. C. Gossard and H. Kroemer, Far-infrared photoresponse of the InAs–GaInSb superlattice, *Appl. Phys. Lett., 59* (7) (1991) 846.
165 D. L. Smith and C. Mailhiot, Strained Type II superlattices, *Surf. Sci., 196* (1988) 683.
166 M. D. Williams and T. H. Chiu, The effect of strain on the valence band structure of InAs (100), *J. Vac. Sci. Technol., B8* (4) (1990) 758.
167 S. Hong, J. P. Loehr, J. E. Oh, P. K. Bhattacharya and J. Singh, Calculations of the electric field dependent far-infrared absorption spectra in InAs–AlGaSb quantum wells, *Appl. Phys. Lett., 55* (9) (1989) 888.
168 H. Mani, A. Joullie, A. M. Joullie, B. Girault and C. Alibert, Band-gap and spin-orbit splitting of the lattice-matched GaAsSb–InAs system, *J. Appl. Phys., 61* (5) (1987) 2101.
169 K. Kudo, J. S. Lee, K. Tanaka, Y. Makita and A. Yamada, Fabrication and characterization of MBE grown InAs–GaAs strained-layer superlattices on variously oriented substrates, *J. Cryst. Growth, 111* (1991) 402.
170 H. Toyoshima, T. Anan, K. Nishi, T. Ichihashi and A. Okamoto, Growth by molecular beam epitaxy and characterization of $(InAs)_m (GaAs)_m$ short period superlattices on InP substrates, *J. Appl. Phys., 68* (3) (1990) 1282.
171 M. Yano, K. Yoh, T. Iwanwaki, Y. Iwai and M. Inoue, Structural stability of ultrathin InAs–GaAs quantum wells grown by migration epitaxy, *J. Cryst. Growth, 111* (1991) 397.
172 S. A. Chalmers, H. Kroemer and A. C. Gossard, The growth of (Al, Ga)Sb tilted superlattices and their heteroepitaxy with InAs to form corrugated-barrier quantum wells, *J. Cryst. Growth, 111* (1991) 647.
173 T. Akazaki, T. Kawakami and J. Nitta, Epitaxial InAs-coupled superconducting junctions, *J. Appl. Phys., 66* (12) (1989) 6121.
174 C. Nguyen, J. Werking, H. Kroemer and E. L. Hu, InAs–AlSb quantum well as superconducting weak link with high critical current density, *Appl. Phys. Lett., 57* (1) (1990) 87.
175 J. R. Söderström, D. H. Chow and T. C, McGill, Demonstration of large peak-to-valley current ratios in InAs–AlGaSb–InAs single-barrier heterostructures, *Appl. Phys. Lett., 55* (13) (1989) 1348.
176 D. Z. -Y. Ting, E. T. Yu, D. A. Collins, D. H. Chow and T. C. McGill, Modeling of novel heterojunction tunnel structures, *J. Vac. Sci. Technol., 8* (4) (1990) 810.
177 L. F. Luo, R. Beresford and W. I. Wang. Resonant tunneling in AlSb–InAs–AlSb double-barrier heterostructures, *Appl. Phys. Lett., 53* (23) (1988) 2320.
178 K. F. Longenbach, L. F. Luo, S. Xin and W. I. Wang, Resonant tunneling in polytype InAs–AlSb–GaSb heterostructures, *J. Cryst. Growth, 111* (1991) 651.
179 J. F. Chen, L. Yang, M. C. Wu, S. N. G. Chu and A. Y. Cho, Studies of the tunneling currents in the InAs–AlSb–GaSb single-barrier interband tunneling diodes grown on GaAs substrates, *J. Cryst. Growth, 111* (1991) 659.
180 U. Kunze, Coherent Zener tunneling in InAs electron inversion layers, *Appl. Phys. Lett., 54* (22) (1989) 2213.